Article

Neuron

A Labeled-Line Neural Circuit for Pheromone-Mediated Sexual Behaviors in Mice

Highlights

- Sex pheromone information is sorted by the amygdala in a sexually dimorphic manner
- A novel pathway from the hypothalamus to midbrain modulates female sexual behavior
- Sex pheromone and predator cue signals are represented by mostly distinct neurons

Authors

Kentaro K. Ishii, Takuya Osakada, Hiromi Mori, Nobuhiko Miyasaka, Yoshihiro Yoshihara, Kazunari Miyamichi, Kazushige Touhara

Correspondence

amiyami@mail.ecc.u-tokyo.ac.jp (K.M.), ktouhara@mail.ecc.u-tokyo.ac.jp (K.T.)

In Brief

Ishii et al. show a labeled-line neural circuitry for a sex pheromone, ESP1, that controls sexual receptivity of female mice. This circuit relays information in a sexually dimorphic manner, which is in line with the sex-dependent effects of ESP1.

Ishii et al., 2017, Neuron *95*, 123–137
July 5, 2017
http://dx.doi.org/10.1016/j.neuron.2017.05.038

CellPress

Neuron
Article

A Labeled-Line Neural Circuit for Pheromone-Mediated Sexual Behaviors in Mice

Kentaro K. Ishii,[1,2,4] Takuya Osakada,[1,2,4] Hiromi Mori,[1,2] Nobuhiko Miyasaka,[3] Yoshihiro Yoshihara,[2,3] Kazunari Miyamichi,[1,2,4,*] and Kazushige Touhara[1,2,5,*]
[1]Department of Applied Biological Chemistry, Graduate School of Agricultural and Life Sciences
[2]ERATO Touhara Chemosensory Signal Project, JST
The University of Tokyo, Tokyo 113-8657, Japan
[3]RIKEN Brain Science Institute, Wako, Saitama 351-0198, Japan
[4]These authors contributed equally
[5]Lead Contact
*Correspondence: amiyami@mail.ecc.u-tokyo.ac.jp (K.M.), ktouhara@mail.ecc.u-tokyo.ac.jp (K.T.)
http://dx.doi.org/10.1016/j.neuron.2017.05.038

SUMMARY

In mice, various instinctive behaviors can be triggered by olfactory input. Despite growing knowledge of the brain regions involved in such behaviors, the organization of the neural circuits that convert olfactory input into stereotyped behavioral output remains poorly understood. Here, we mapped the neural circuit responsible for enhancing sexual receptivity of female mice by a male pheromone, exocrine gland-secreting peptide 1 (ESP1). We revealed specific neural types and pathways by which ESP1 information is conveyed from the peripheral receptive organ to the motor-regulating midbrain via the amygdala-hypothalamus axis. In the medial amygdala, a specific type of projection neurons gated ESP1 signals to the ventromedial hypothalamus (VMH) in a sex-dependent manner. In the dorsal VMH, which has been associated with defensive behaviors, a selective neural subpopulation discriminately mediated ESP1 information from a predator cue. Together, our data illuminate a labeled-line organization for controlling pheromone-mediated sexual behavioral output in female mice.

INTRODUCTION

Animals detect diverse environmental signals to adjust their behaviors. In most cases, this process requires learning, and the animal gradually acquires a proper response to a sensory input by utilizing a plastic neural circuit. On the contrary, some sensory signals innately instruct a stereotyped behavioral response, even on first contact. These include various instinctive behaviors such as mating, aggression, and defensive behaviors, which can be robustly evoked by signals from a partner, competitor, or predator, respectively. However, little is known about the neural basis that allows the animal to select the appropriate behavioral output for a particular sensory input. The key to solving this question is identifying the exact neural circuit that conveys information about a sensory signal with a behavioral impact, from the periphery to the behavioral centers in the brain.

For many animals, including mice, the vomeronasal system is critical for detecting chemical signals that control instinctive behaviors (Touhara and Vosshall, 2009). In this system, the vomeronasal receptors expressed in vomeronasal sensory neurons (VSNs) detect chemical and protein cues. This information is first relayed to the accessory olfactory bulb (AOB) and then to the third-order neurons in the medial amygdala (MeA), posteromedial cortical amygdala (PMCo), and bed nucleus of the stria terminalis (BNST) (Dulac and Wagner, 2006). These neurons then send their axonal projections to broad hypothalamic areas where various instinctive behaviors are thought to be controlled. For instance, in mice, the dorsal part of ventromedial hypothalamus (VMHd) regulates defensive behaviors against predators (Canteras, 2002; Kunwar et al., 2015; Silva et al., 2013; Wang et al., 2015), whereas the ventrolateral VMH (VMHvl) is critical for aggression and sexual behaviors in male mice (Lee et al., 2014; Lin et al., 2011; Yang et al., 2013). The VMHvl is also crucial for female sexual behaviors, especially lordosis response, a typical male-receptive posture (Pfaff and Sakuma, 1979; Yang et al., 2013). Additionally, another hypothalamic area, the medial preoptic area (MPA), is related to pup-directed aggression, parenting, and mating behaviors in male mice and maternal behaviors in female mice (Lonstein and Gammie, 2002; Tsuneoka et al., 2015; Wu et al., 2014).

Despite the emerging understanding of the sensory signals and brain areas that control instinctive behaviors, an important unresolved question is the neural organization that converts sensory input into an appropriate behavioral output. The major obstacle to answering this question is the complexity of the signals; physiologically relevant signals often consist of multiple chemicals, which are received by many receptors and therefore may be processed by diverse brain regions. In contrast, in our previous studies, we established a simpler model. Exocrine gland-secreting peptide 1 (ESP1), which is purified from the lacrimal gland of male mice (Kimoto et al., 2005), is detected by a single member of vomeronasal receptor type 2 family, V2Rp5 (also known as Vmn2r116) and enhances female lordosis behavior (Haga et al., 2010). This makes ESP1 a powerful model

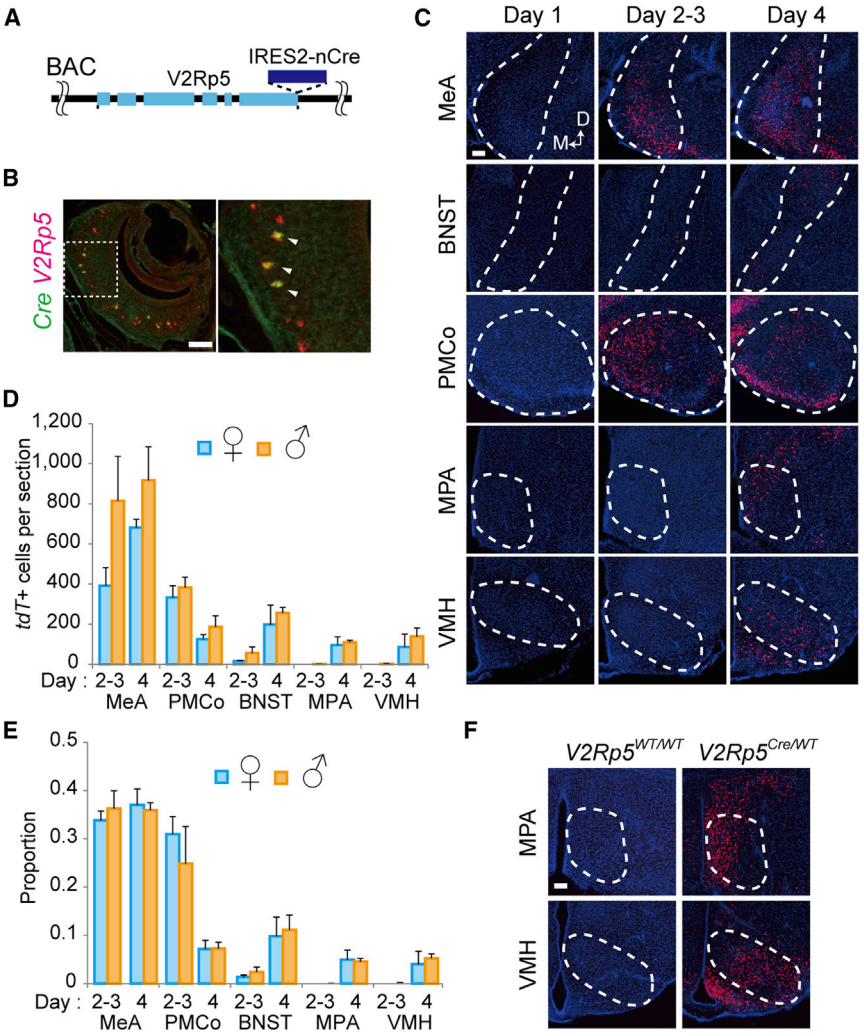

Figure 1. Sequential Anterograde Circuit Mapping from V2Rp5-Expressing Sensory Neurons

(A) Construct of the bacteria artificial chromosome (BAC) transgene.

(B) A representative section showing *Cre* (green) and *V2Rp5* (red) mRNA expression in the VNO of *V2Rp5-Cre* transgenic mouse. White arrowheads indicate *Cre*+ *V2Rp5*+ VSNs.

(C) Representative coronal sections showing tdT+ cells (red) 1, 2–3, or 4 days after HSV infection.

(D and E) Number of tdT+ cells per section (D) or the proportion of tdT+ cells (E) in each area normalized to total tdT+ cells in all counted areas 2–3 days or 4 days after HSV infection. 2–3 days, n = 5 animals each. 4 days, female, n = 3, male, n = 4.

(F) Representative coronal sections showing tdT+ cells in the VMH and MPA of heterozygous *V2Rp5-Cre* transgenic mice ($V2Rp5^{Cre/WT}$) and wild-type (WT) littermates ($V2Rp5^{WT/WT}$) 6 days after HSV infection.

Error bars, SEM. Scale bars, 100 μm. MeA, medial amygdala; PMCo, posteromedial cortical amygdala; BNST, bed nucleus of stria terminalis; MPA, medial preoptic area; VMH, ventromedial hypothalamus. See also Figure S1 for additional data.

to study the basic principles that convert sensory input to behavioral output. Additionally, the same pheromone, in conjunction with unfamiliar male urine, was shown to enhance inter-male aggression when introduced to adult male mice (Hattori et al., 2016), allowing us to further study sex-specific information processing in the brain. By combining various viral and genetic tools, histochemical analysis, and behavioral assays, we show that a labeled-line neural circuit from the peripheral sensory organ to the hypothalamus is dedicated to sex-pheromone-mediated behavior in mice.

RESULTS

Sequential Anterograde Circuit Mapping from a Single Vomeronasal Sensory Channel

To elucidate the anatomical basis upon which ESP1 signals are represented in higher brain regions, we mapped the downstream neural circuits of V2Rp5-expressing VSNs using the H129 strain of herpes simplex virus (HSV-H129ΔTK-TT) (Lo and Anderson, 2011). This viral tracer, upon activation by Cre recombinase, spreads anterogradely from neuron to neuron and labels infected cells with tdTomato. To restrict the initial viral activation to only V2Rp5-expressing VSNs, we generated transgenic mice expressing Cre under the control of the *V2Rp5* regulatory sequence (*V2Rp5-Cre*; Figure 1A). Two-color *in situ* hybridization (ISH) using *Cre* and *V2Rp5* probes showed that 22% (21 out of 94 observed cells) of *V2Rp5*+ VSNs co-expressed *Cre*, whereas all *Cre*+ VSNs co-expressed *V2Rp5* in *V2Rp5-Cre* mice (21 out of 21 observed cells) (Figure 1B). No Cre expression was found in the AOB or higher brain regions that receive input from the AOB (data not shown).

We next transduced VSNs with H129ΔTK-TT from their axonal termini at the AOB (Lo and Anderson, 2011) and analyzed the brain 1–4 days after viral infection. 1 day after viral infection, *tdTomato*-positive (tdT+) cells were not observed in the higher brain region (Figures 1C and S1A). At 2–3 days after viral injection, we detected tdT+ cells in the MeA, PMCo, and BNST, whereas hypothalamic regions such as the VMH and MPA remained unlabeled (Figures 1C–1E and S1A), supporting previous data showing that the MeA, PMCo, and BNST are the major direct synaptic targets of AOB mitral cells (Dulac and Wagner, 2006). 4 days after viral injection, we started to observe tdT+ cells in various brain regions including the VMH and MPA (Figures 1C–, S1A, and S1B), which suggests that these hypothalamic regions are downstream of the MeA, PMCo, and/or BNST. No apparent difference was found in the number or spatial distribution of tdT+ cells between male and female mice (Figures 1D and 1E), even in the areas where previous data

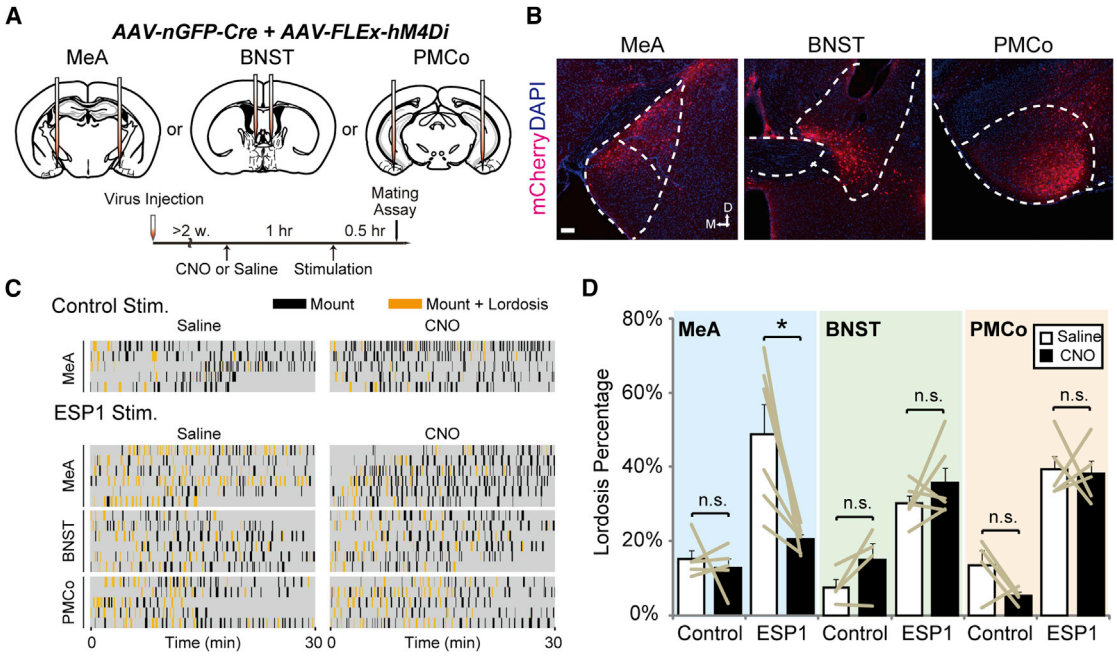

Figure 2. The Medial Amygdala is Necessary for ESP1-Mediated Enhancement of Lordosis in Female Mice

(A) Schematic of the experimental setup and time line of procedures. *AAV-nGFP-Cre* and *AAV-FLEx-hM4Di* were injected into the MeA, BNST, or PMCo of wild-type female mice.

(B) Representative coronal sections showing expression of hM4Di (mCherry+ shown in red) in each area. DAPI staining is shown in blue. The number of infected cells per square millimeter was calculated as follows: MeA, 177 ± 21, n = 11 animals; BNST, 200 ± 28, n = 10; PMCo, 266 ± 68, n = 9 (mean ± SEM). Scale bar, 100 μm.

(C) Raster plots of behavior episodes during the mating assay. Mounting episodes with or without a lordosis response by female mice are shown in orange and black bars, respectively.

(D) The lordosis percentage (defined by the number of mounting episodes with lordosis divided by the total number of mounting episodes) following i.p. injection of saline (average shown as white bar graph) or CNO (black bar graph). Gray lines represent trials from individual animals. Error bars, SEM. n = 4–6 animals. Paired Student's t test with Bonferroni correction. *p < 0.05. n.s., not significant.

showed sexually dimorphic activation patterns following ESP1 exposure (Haga et al., 2010). This may suggest that HSV transduces any synaptic connection regardless of its functional property. Control experiments using wild-type littermates showed no tdT+ cells throughout the brain (Figure 1F). Together, this anterograde transneural tracing originated from V2Rp5-expressing VSNs established that ESP1 information is sequentially conveyed from the third-order neurons in the MeA, BNST, and PMCo to broad fourth-order neurons in the hypothalamic regions. We next functionally dissected these higher brain areas by using behavioral output (enhancement of lordosis) in female mice as a readout.

The MeA Is Necessary for ESP1-Mediated Enhanced Lordosis in Female Mice

To determine the necessity of third-order neurons in the MeA, BNST, and PMCo for ESP1-mediated enhancement of lordosis, we virally targeted hM4Di, a pharmaco-genetic neural inhibitor (Armbruster et al., 2007), to each brain area (Figures 2A and 2B). After recovery from viral injection, we observed the animal's sexual behavior after exposure to ESP1. Consistent with the previous report (Haga et al., 2010), female mice pre-stimulated with ESP1 exhibited an 2- to 2.5-fold greater percentage of lordosis compared to females pre-exposed to a control stimulus (saline injection) (Figures 2C and 2D). This enhanced lordosis was disrupted by silencing the MeA neurons via intraperitoneal (i.p.) injection of clozapine N-oxide (CNO), whereas ESP1-independent basal lordosis was intact. In contrast, blocking neural activities in the BNST or PMCo did not affect ESP1-mediated lordosis enhancement or basal lordosis per se. These data demonstrate that the MeA is necessary for ESP1-mediated enhanced lordosis in female mice.

Sexually Dimorphic Sorting of ESP1 Information in the MeA

The MeA can be divided into three subregions (the anterior [MeAa], posterodorsal [MeApd], and posteroventral [MeApv] areas) based on anatomical landmarks. The MeApd is thought to be related to social behaviors, whereas the MeApv is thought to relay information about defensive stimuli to the hypothalamus (Choi et al., 2005; Newman, 1999). Thus, we speculated that the sex pheromone ESP1 would activate MeApd. However, by analyzing the spatial distribution of *cFos*+ cells in the MeA, we found that the MeApv, but not the MeApd, showed the strongest *cFos*+ induction upon ESP1 exposure in both sexes (Figures 3A, 3B, and S2A–S2D). Within the MeApv, no major difference was observed in the fraction of excitatory neurons activated by ESP1 between sexes (Figure S2E and S2F). We noticed a small

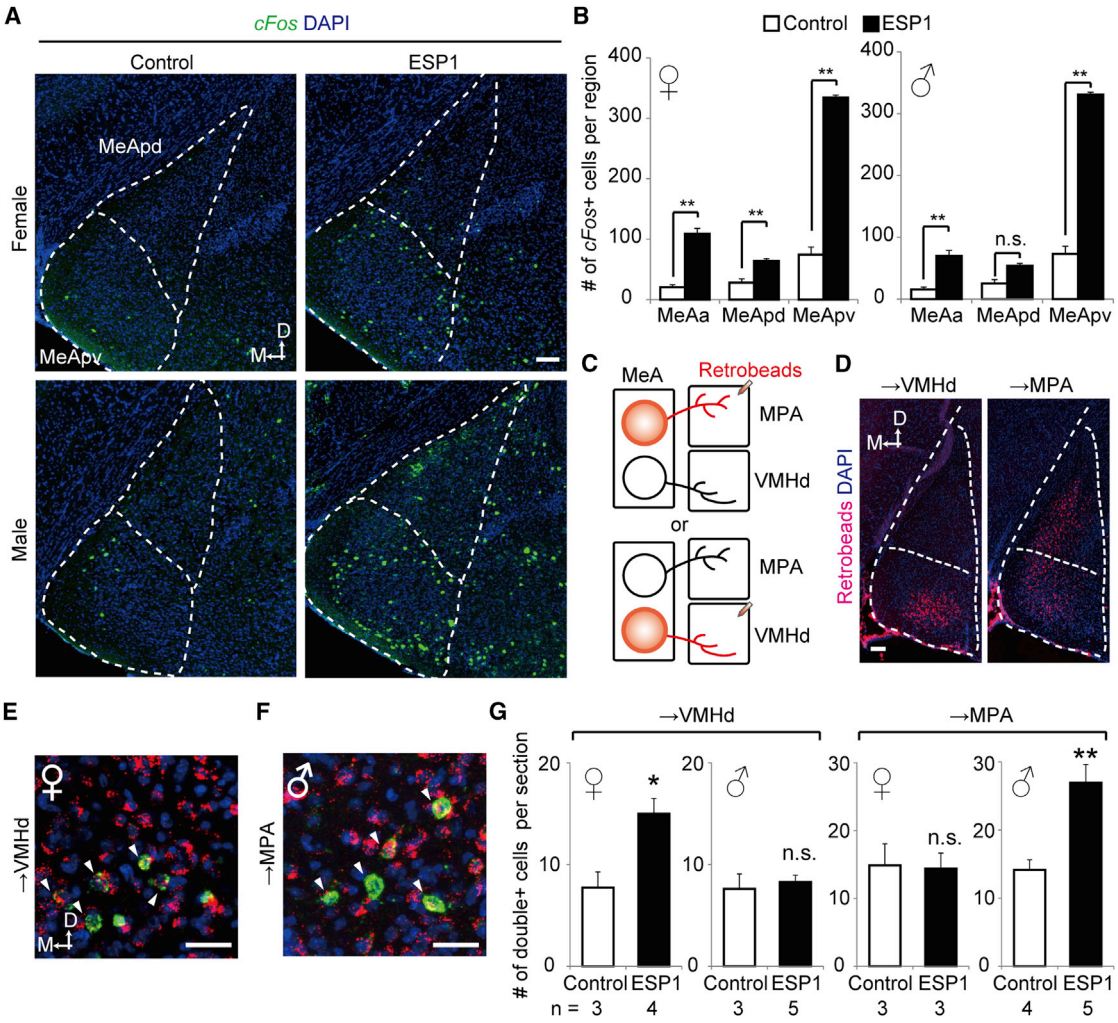

Figure 3. Sexually Dimorphic Sorting of ESP1 Information by the MeApv

(A) Representative coronal sections showing *cFos* mRNA expression (green) in the MeA of mice exposed to ESP1 or a control stimulus.

(B) Number of *cFos*+ cells in the anterior MeA (MeAa), MeApd, and MeApv of mice exposed to ESP1 (black) or the control (white) in female (left) and male (right) mice. n = 4 for ESP1 and n = 5 for control (females); n = 3 each for ESP1 and control (males). Student's t test with Bonferroni correction, $^{**}p < 0.01$.

(C) Schematic of the experimental setup for projection-specific labeling. Retrobeads were injected into either the VMHd or MPA.

(D) Representative coronal sections showing labeled VMHd projectors (→VMHd) and MPA projectors (→MPA) in the MeA.

(E and F) Representative coronal sections showing *cFos* expression in VMHd-projectors of female mice (E) and MPA-projectors of male mice (F) following ESP1 exposure. White arrowheads indicate Retrobeads+ cells expressing *cFos*.

(G) Number of *cFos*+ and beads+ cells per section in female or male mice (left, VMHd projectors, right, MPA projectors). The number of animals is noted below each graph. Student's t test, $^{*}p < 0.05$, $^{**}p < 0.01$.

Error bars, SEM. D, dorsal, M, medial. Scale bars, 100 μm. See also Figures S2 and S5 for additional data.

but significant increase in the number of *cFos*+ cells in the MeApd only in females (Figures 3B and S2A).

Previous studies have shown that two hypothalamus areas downstream of the MeA, the VMH and MPA, were activated after ESP1 exposure (Haga et al., 2010). Thus, we next aimed to identify the excitatory projection neurons that send ESP1 information to the VMH and MPA. We labeled neurons that project to these areas by injecting a retrograde tracer, red Retrobeads, into each target (Figure 3C). We found that neurons projecting to the VMHd (VMHd projectors) were located mainly in the MeApv, but not in MeApd, while neurons projecting to the MPA (MPA projectors) were in both the MeApd and the MeApv (Figure 3D). Importantly, the majority of the projection neurons in the MeApv were glutamatergic (Figures S2G and S2H). Thus, we next tested whether VMHd and MPA projectors in the MeApv are activated by ESP1 and, if so, whether they are activated differently in males and females. In female mice, ESP1 significantly induced *cFos* mRNA expression in VMHd projectors, but not in MPA projectors (Figures 3E and 3G). The induction pattern was opposite in male mice, in which ESP1 induced *cFos* mRNA in MPA projectors, but not in VMHd projectors (Figures 3F and 3G). These data suggest a model in which MeApv

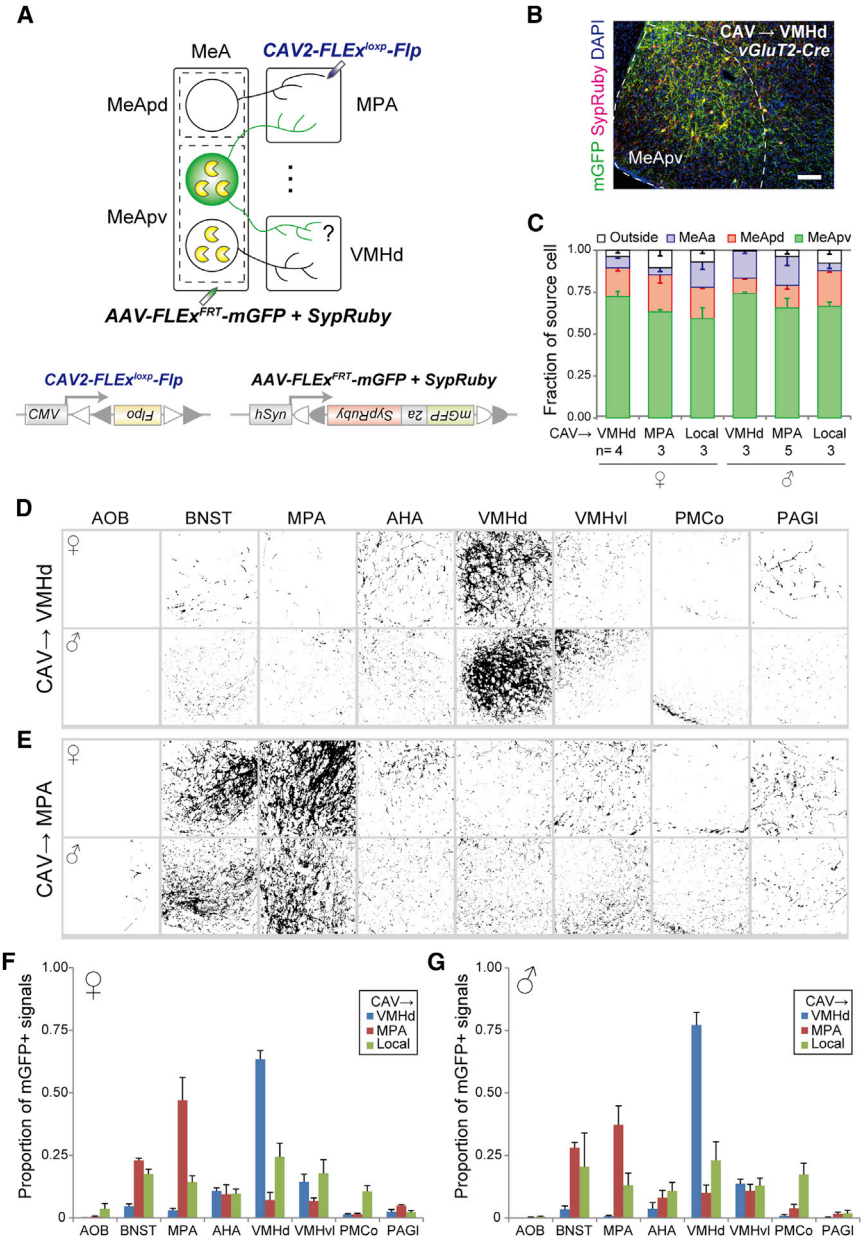

Figure 4. VMHd and MPA Projectors in the MeApv Have Distinct Axonal Arborization Patterns

(A) Schematic of the experimental setup. (Top) *CAV2-FLEx^{loxp}-Flp* was injected into either the VMHd or MPA. *AAV-FLEx^{FRT}-mGFP* was injected into the MeApv. Yellow Pac-Man symbols represent Cre expression in *vGluT2-Cre* mice. (Bottom) Schematic drawing of the CAV2 and AAV constructs.

(B) A representative coronal section showing mGFP and SypRuby expression in MeApv neurons after *CAV2* injection into the VMHd and AAV injection into the MeApv. Scale bar, 100 μm.

(C) Fraction of source cells (defined by the expression of mGFP) in the MeApd (red), MeApv (green), MeAa (purple), or outside the MeA (white) in each injection condition. The number of animals for each condition is shown at the bottom.

(D and E) Representative images of binarized mGFP signals of a coronal section across eight brain regions collected from animals labeled with VMHd projector (D) or MPA projector (E).

(F and G) Proportion of total axon arborization of VMHd projectors, MPA projectors, and pan-MeApv *vGluT2*+ neurons across eight brain regions in females (F) and males (G).

Error bars, SEM. AOB, accessory olfactory bulb; BNST, bed nucleus of stria terminalis anterior domain; MPA, medial preoptic area; AHA, anterior hypothalamus; VMHd and VMHvl, dorsomedial and ventrolateral ventromedial hypothalamus; PMCo, posteromedial cortical amygdala; PAGl, lateral periaqueductal gray. See also Figure S3.

neurons sort ESP1 information to the VMHd in female mice and to the MPA in male mice.

VMHd and MPA Projectors in the MeApv Have Distinct Axonal Arborization Patterns

Findings from the retrograde-tracer-mediated analysis suggest the presence of pathway-specific projection neurons in the MeApv that send axons preferentially to either the VMHd or the MPA. To directly visualize and characterize them, we next analyzed the output structure of VMHd and MPA projectors in the MeApv utilizing a canine adenovirus type 2 (CAV2)-mediated strategy to visualize axonal arbors (Schwarz et al., 2015). Because VMHd and MPA projectors in the MeApv were predominantly glutamatergic neurons that express vesicular glutamate transporter type 2 (*vGluT2*) (Figures S2G and S2H), we used *vGluT2-IRES-Cre* (*vGluT2-Cre*; Vong et al., 2011) mice to specifically label MeApv projection neurons. We virally targeted *CAV-FLEx^{loxp}-Flp*, a CAV2 variant that retrogradely expresses Flp recombinase in a Cre-dependent manner, to either the VMHd or the MPA of *vGluT2-Cre* mice. Local injection of a Flp-dependent adeno-associated virus (AAV)-expressing membrane-tethered GFP and synapse-localized mRuby (*AAV-FLEx^{FRT}-mGFP*; Beier et al., 2015) into the MeApv allowed us to visualize the axons and pre-synaptic terminals of VMHd and MPA projectors (Figure 4A). As a control, we injected a mixture of *CAV-FLEx^{loxp}-Flp* and *AAV-FLEx^{FRT}-mGFP* into the MeApv to indiscriminately label MeApv projection neurons without prior selection of the target.

In all cases, more than 60% of the mGFP-expressing neurons were located in the MeApv (Figures 4B and 4C). Quantification of mGFP signals in eight broad brain regions revealed that the axonal arbors of VMHd projectors were highly localized in the VMHd (Figure 4D). In contrast, axonal arbors of MPA projectors were sparse in the VMHd and dense in the MPA and BNST (Figure 4E), suggesting that VMHd and MPA projectors

are relatively specific in terms of their projection patterns and composed of mostly distinct populations. We did not observe major differences in the arborization patterns of VMHd or MPA projectors between male and female mice (Figures 4F, 4G, S3A, and S3B). Additionally, we found no differences in the proportion of axonal arbors in the VMHd or MPA between male and female mice as revealed by labeling of pan-*vGluT2*+ neurons when CAV2 was injected locally into the MeApv (Figures 4F and 4G, green bars), indicating that the output structure of the MeApv is sexually monomorphic. This conclusion was further supported by the fact that the numbers of VMHd and MPA projectors per section labeled by Retrobeads (Figures 3C and 3D) were similar between sexes (VMHd, female: 173 ± 16, mean ± SEM, n = 10, male: 203 ± 21, n = 12. MPA, female: 280 ± 30, n = 10, male: 292 ± 32, n = 9.). Of note, these observations were confirmed by analyzing signals at the synaptic termini, where the number of SypRuby signals showed a high correlation with the density of mGFP (Figures S3C–S3E).

In sum, data from Figures 3 and 4 indicate that ESP1 information is conveyed from the MeApv to the downstream hypothalamic areas by a common output structure used differently depending on the sex of the recipient mice. ESP1 specifically activates VMHd projectors in female and MPA/BNST projectors in males, which may underlie the sexually dimorphic activation of distinct hypothalamic areas by ESP1.

vGluT2+ Neurons in the MeApv Are Necessary for Sexual Behavior Enhancement by ESP1

To further confirm the importance of *vGluT2*+ MeApv neurons for ESP1 information processing, we silenced their neural activities by virally targeting hM4Di into the MeA of *vGluT2-Cre* female mice. This approach enabled us to express hM4Di mainly in the MeApv (Figures 5A–5C). Activating hM4Di by CNO i.p. injection reduced the number of *cFos*+ cells in the MeA after ESP1 exposure in female mice, validating that hM4Di inactivates MeA neurons (Figures 5D and 5E). Of note, this quantification included *cFos*+ GABAergic neurons, which were not manipulated in this experiment but were activated after ESP1 stimulation (Figures S2E and S2F). This may underlie relatively minor reduction of ESP1-responding neurons in the MeA.

In the classical view, the VMHd is the center of defensive behaviors evoked by various predator cues (Canteras, 2002), whereas VMHvl neurons are thought to regulate female sexual behavior (Yang et al., 2013). According to this model, a sex pheromone should activate the VMHvl. In contrary to this prediction, by analyzing distribution of *cFos*+ cells within VMH, we found that VMHd was activated by ESP1. Notably, this ESP1-induced *cFos*+ expression within VMHd was significantly reduced by silencing *vGluT2*+ MeApv neurons (Figures 5F and 5G), demonstrating that MeApv → VMHd pathway mediates ESP1 information in female mice.

This silencing of *vGluT2*+ MeApv neurons resulted in significant disruption of ESP1-mediated enhancement of lordosis without affecting the basal lordosis level (Figure 5H and 5I), similar to the finding shown in Figure 2D in which the type of neurons for inactivation was not regulated. In the control stimulation group, no significant difference was found after CNO i.p. injection. Collectively, these data suggest that *vGluT2*+ MeApv is necessary for ESP1-mediated enhanced sexual behavior, although we did not exclude the possibility that *vGluT2*+ neurons in MeAa and/or MeApd may also contribute to the processing of ESP1 information.

SF1+ Neurons in the VMHd Are Necessary for Sexual Behavior Enhancement by ESP1

We next asked if the activation of the VMHd by ESP1 indeed mediates enhancement of lordosis in female mice. Steroidogenic factor 1 (*SF1*), an orphan nuclear receptor gene, is a specific gene marker of the majority of VMHd neurons (Ikeda et al., 1995). Two-color ISH for *cFos* and *SF1* revealed significant induction of *cFos* in *SF1*+ VMHd neurons, but not in *SF1*− VMHd neurons or VMHvl neurons (Figures 6A and 6B). In ESP1 stimulated animals, 83% ± 1% of *cFos*-expressing neurons in the VMHd co-expressed *SF1*.

To determine the necessity of *SF1*+ neurons for ESP1-mediated enhancement of lordosis in female mice, we genetically ablated *SF1*+ neurons by bilaterally injecting the AAV expressing diphtheria toxin subunit A (DTA) in a Cre-dependent manner (*AAV-FLEx-DTA*) into the VMHd of *SF1-Cre* transgenic mice (Dhillon et al., 2006) (Figure 6C). We observed a drastic elimination of *SF1*+ neurons in the VMHd of *SF1::DTA* mice compared to animals that received injection of control virus expressing GFP (Figure 6D). Of note, the surrounding VMHvl area was unaffected by this procedure, based on normal marker gene expression (data not shown). *SF1::DTA* mice pre-exposed to ESP1 showed a marked reduction in the enhancement of the percentage of lordosis by ESP1, whereas ESP1-independnet basal lordosis was intact (Figures 6E and 6F).

We also inhibited neural activities of *SF1*+ neurons by bilaterally injecting *AAV-FLEx-hM4Di* or *AAV-FLEx-GFP* as control into the VMHd of *SF1-Cre* female mice (Figure 6G). We found that the infected cells were restricted in the VMHd (Figure 6H). Mice injected with *AAV-FLEx-hM4Di* (*SF1::hM4Di*) received an i.p. injection of CNO 1 hr before ESP1 exposure to observe the effect of inhibition of *SF1*+ neurons. *SF1::hM4Di* mice, similar to *SF1::DTA* mice, showed basal lordosis, but ESP1-mediated enhancement of lordosis was reduced to a level similar to that of control stimulus-exposed mice (Figure 6J). In additional control experiments, *SF1-Cre* mice injected with an AAV expressing GFP in a Cre-dependent manner (*SF1::GFP*) exhibited ESP1-mediated enhanced lordosis in the presence of CNO, ruling out the possibility that CNO impairs processing of ESP1. We observed a negative correlation between the number of infected cells in the VMHd and the lordosis percentage in CNO i.p. trials in *SF1::hM4Di* ESP1-stimulated animals (Figure 6K). Taken together, we conclude that *SF1*+ neurons are necessary for ESP1-mediated enhancement of lordosis in female mice.

Notably, this loss-of-function phenotype of *SF1*+ neurons in the VMHd was considerably different from that of VMHvl neurons that expressed estrogen receptor alpha (*Esr1*). Although genetic ablation of *SF1*+ VMHd neurons had no effect on basal lordosis, genetic ablation of *Esr1*+ VMHvl neurons using *Esr1-2A-Cre* (*Esr1-Cre*) mice (Lee et al., 2014) resulted in severe defects in basal lordosis (Figure S4), consistent with previous studies (Yang et al., 2013). This suggests different roles for the VMHd and VMHvl in the sexual behaviors of females: the VMHd is

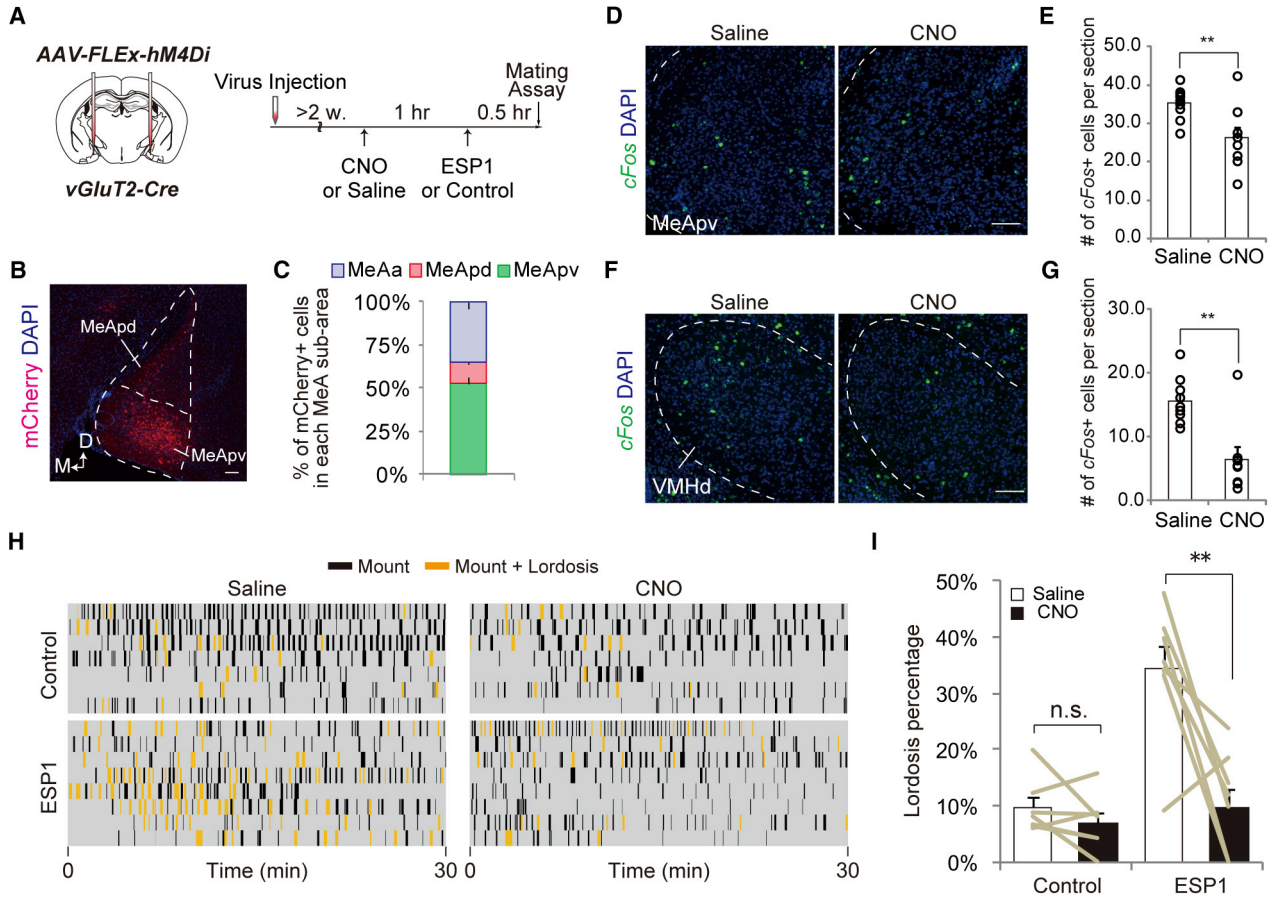

Figure 5. *vGluT2*+ MeApv Neurons Are Necessary for Sexual Behavior Enhancement by ESP1

(A) Schematic of the experimental setup. *AAV-FLEx-hM4Di* was injected into the MeA of female *vGluT2-Cre* mice. Animals were intraperitoneally injected with CNO or saline as control 1 hr before ESP1 or control stimulation.

(B) Representative coronal section showing expression of hM4Di (mCherry+ shown in red). DAPI staining is shown in blue. Scale bar, 100 μm. 154 ± 33 mCherry+ cells per square millimeter, n = 15 animals.

(C) Proportion of mCherry+ cells in MeAa (purple), MeApd (red) and MeApv (green) among the entire MeA. N = 30 unilateral MeA.

(D and F) Representative coronal sections showing expression of *cFos* mRNA (green) in MeApv (D) and VMHd (F). Animals were intraperitoneally injected with CNO or saline as control 1 hr before ESP1 stimulation. Brain samples were collected 30 min after ESP1 stimulation.

(E and G) Number of *cFos*+ cells per section in a unilateral MeA (E, n = 9 unilateral MeA each) and VMH (G, saline, n = 10 unilateral VMH, CNO, n = 8) of CNO or saline intraperitoneally injected animals. Student's t test, $^{**}p < 0.01$.

(H) Raster plots of behavior episodes during the mating assay as in Figure 2C.

(I) Lordosis percentage following i.p. injection of saline (average shown as white bars) or CNO (black bars). Control, n = 7 animals, ESP1 stimulus, n = 8. Paired Student's t test with Bonferroni correction.

Error bars, SEM. D, dorsal, M, medial.

involved in the enhancement of lordosis, and the VMHvl is involved in basal lordosis.

ESP1-Responding Neurons in the VMHd Are Sufficient to Enhance Lordosis

Our data, in conjunction with data from others, suggested that the VMHd functions both in defensive behaviors and ESP1-mediated enhanced lordosis. We next asked how this functional heterogeneity is represented within the VMHd and if the activity of VMHd neurons is sufficient to enhance female sexual behavior. To address these questions, we first compared the neural representation of ESP1 within the VMHd with that of a predator cue contained in the skin shed from a snake. Snakeskin evokes defensive risk assessment behaviors in mice in a manner that depends on the function of the vomeronasal system (Papes et al., 2010). We confirmed that snakeskin activated VMHd projectors in the MeApv in both sexes and did not enhance sexual behavior in female mice (Figures S5A and S5B).

We then conducted cellular compartment analysis of temporal activity with fluorescent ISH (catFISH) (Guzowski et al., 1999; Lin et al., 2011) to compare the neural population that is activated by two sequential stimuli in a single animal. Animals sacrificed 5 min after the stimulation had exclusively nuclear transcripts of the immediate early gene *Nr4a1* (Maxwell and Muscat, 2006), whereas those sacrificed 45 min after the stimulation had only cytoplasmic transcripts (Figure 7A). We observed that in animals

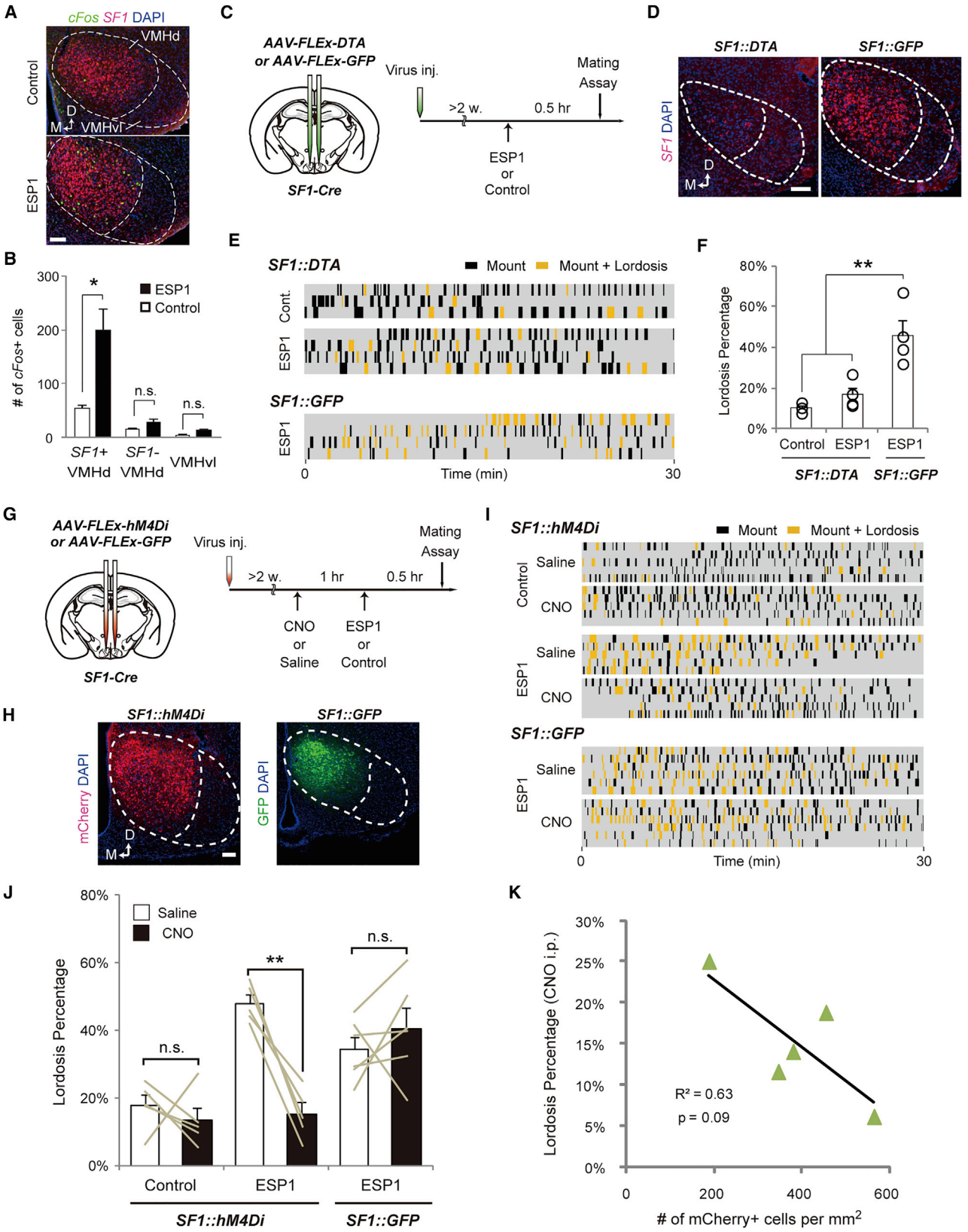

(legend on next page)

that received the same stimulus twice, nearly 80% of the cells expressing *Nr4a1* transcripts in the nuclei also expressed cytoplasmic *Nr4a1* mRNA. In contrast, in animals that received different stimuli, less than 30% of the cells exhibited nuclear and cytoplasmic transcripts, indicating that ESP1 and snakeskin activated mostly non-overlapping neural populations in the VMHd (Figures 7A and 7B). We obtained similar results in the regions upstream of the VMHd, namely, the AOB and MeApv (Figures S5C–S5F). These data suggest the presence of parallel dedicated pathways for ESP1 and predator cue information within the vomeronasal system.

Next, we examined whether the activation of ESP1-responding neurons in the VMHd is sufficient for enhancing lordosis in female mice. We used the method of targeted recombination in active populations (TRAP) (Guenthner et al., 2013), which allows genetic access to neurons that are active during a specific time window determined by tamoxifen administration. We first injected the bilateral VMHd of *Arc-CreER* mice with an AAV expressing pharmaco-genetic neural activator hM3Dq (Armbruster et al., 2007) fused with mCherry (*AAV-FLEx-hM3Dq*) in a Cre-dependent manner (Figure 7C). Each mouse was administered tamoxifen 1 week after the virus injection followed by exposure to ESP1, snakeskin, or no stimulus as a control to express hM3Dq in ESP1-responding, snakeskin-responding, or basally active neurons, respectively. When animals were exposed to ESP1, ESP1-TRAP neurons in the VMH tended to be activated more than snakeskin- and basal activity TRAP neurons (Figures S6A–S6C). This was not the case in nearby structures of the VMH (Figures S6D and S6E). Thus, ESP1-TRAP preferentially labeled ESP1-responding neurons in the VMH, permitting us to activate them to assess the behavioral impact.

More than 2 weeks after tamoxifen administration, CNO was injected i.p. to activate the "TRAPed" neurons 1.5 hr before male entry into the home cage. We observed that activation of ESP1-TRAP neurons significantly enhanced lordosis, which was not observed with activation of snakeskin or basal activity TRAP neurons (Figure 7D). There also seemed to be a positive correlation between the efficiency of labeling ESP1-responding neurons and lordosis percentage in CNO i.p. trials (Figure 7E).

As the temporal and spatial resolution of pharmaco-genetic manipulation is poor, we next utilized an optogenetic activation tool. We injected the unilateral VMH of *Arc-CreER* mice with an AAV expressing channelrhodopsin-2 (ChR2) (Boyden et al., 2005) fused with an enhanced yellow fluorescent protein (eYFP) in a Cre-dependent manner (*AAV-FLEx-ChR2*) followed by placement of an optical fiber above the injection site (Figures 7F, S6F, and S6G). ESP1- or snakeskin-responding neurons were TRAPed as described in hM3Dq-injected animals. Exposure to ESP1 after the mating assay showed that a larger proportion of ChR2-eYFP-expressing neurons co-expressed *cFos* in ESP1-TRAP animals compared to snakeskin-TRAP animals (Figures S6H and S6I). In the mating assay, we observed that 5-min light stimulation of ChR2-expressing ESP1-TRAP neurons 1 hr before male entry significantly increased the percentage of lordosis, which was not observed following light stimulation of snakeskin-TRAP neurons (Figure 7G). Taken together, we conclude that the VMHd contains an ESP1-responding neural subpopulation whose activities are sufficient to enhance sexual behavior. This population is composed of neurons that are intermingled but mostly distinct from those related to defensive behaviors.

The Pathway of *SF1*+ VMHd Neurons to the Dorsal PAG Is Necessary for Sexual Behavior Enhancement by ESP1

We next aimed to identify the downstream region of the VMHd that is necessary for sexual behavior enhancement by ESP1. Long projections of *SF1*+ VMHd neurons innervate various brain regions in the hypothalamus, including the MPA and areas in the midbrain such as the dorsal PAG (PAGd) (Lindberg et al., 2013). A previous study has shown that more than half of *SF1* neurons project their axonal collaterals to multiple brain regions (Wang et al., 2015). We applied the CAV2-mediated strategy to comprehensively analyze the output structure of *SF1* neurons. We compared the distribution of axonal arbors of *SF1*+ PAGd

Figure 6. *SF1*+ VMH Neurons Are Necessary for Sexual Behavior Enhancement by ESP1

(A) Representative coronal sections showing *cFos* (green) and *SF1* (red) expression in the VMHd of female mice exposed to ESP1 or a control stimulus.

(B) Number of *SF1*+, *SF1*−, and VMHvl cells that co-express *cFos* in female mice exposed to ESP1 (black) or the control stimulus (white). n = 4 for ESP1 and n = 5 animals for control stimulus. Student's t test with Bonferroni correction.

(C) Schematic of the experimental setup and timeline of experimental manipulation. *AAV-FLEx-DTA* or *AAV-FLEx-GFP* was injected into the VMHd of female *SF1-Cre* mice.

(D) Representative coronal sections showing *SF1*+ mRNA (red) expression in *AAV-FLEx-DTA*-injected mice (*SF1::DTA*) and *AAV-FLEx-GFP* injected mice (*SF1::GFP*). 245 ± 10 *SF1*+ cells per section in *SF1::GFP* mice, n = 8 unilateral VMHd. 99 ± 24 in *SF1::DTA* mice, n = 14 unilateral VMHd.

(E) Raster plots of behavior episodes during the mating assay as in Figure 2C.

(F) Lordosis percentage of *SF1::DTA* mice exposed to ESP1 or control stimulus, or *SF1::GFP* mice exposed to ESP1. *SF1::DTA*, control, n = 3, ESP1, n = 4. *SF1::GFP,* ESP1, n = 4. One-way ANOVA with Bonferroni correction.

(G) Schematic of the experimental setup and timeline of experimental manipulation. *AAV-FLEx-hM4Di* or *AAV-FLEx-GFP* was injected into the VMHd of female *SF1-Cre* mice.

(H) A representative coronal section showing hM4Di (mCherry+ shown in red) expression in the VMHd of *SF1::hM4Di*, and GFP (shown in green) expression of *SF1::GFP* animals. 396 ± 47 GFP+ cells per square millimeter in *SF1::GFP* mice, n = 6 animals; 414 ± 37 mCherry+ cells in *SF1::hM4Di* mice, n = 10.

(I) Raster plots of behavior episodes during the mating assay.

(J) Lordosis percentage following i.p. injection of saline (average shown as white bars) or CNO (black bars). *SF1::hM4Di*, control, n = 5, ESP1 stimulus, n = 5. *SF1::GFP*, ESP1, n = 6. Paired Student's t test with Bonferroni correction.

(K) Correlation between the number of hM4Di-infected cells per square millimeter (x axis) and the lordosis percentage in CNO i.p. conditions (y axis) of *SF1::hM4Di*, ESP1 animals. n = 5. We noticed a considerable negative correlation (R^2 = 0.63, p = 0. 09), suggesting that efficient inhibition of the *SF1*+ neurons tended to suppress lordosis.

Error bars, SEM. *p < 0.05, **p < 0.01. n.s., not significant. Scale bars, 100 μm. D, dorsal; M, medial. See also Figure S4.

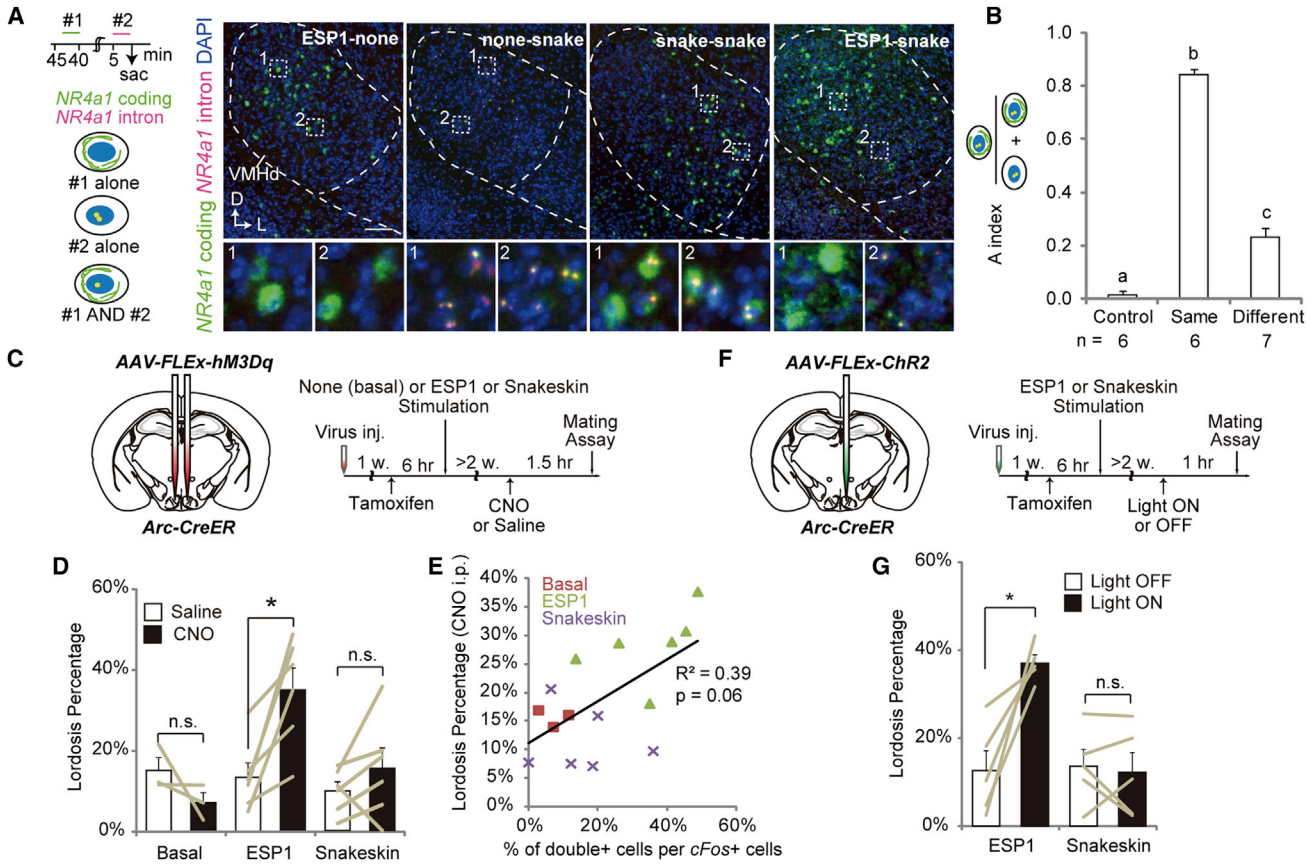

Figure 7. ESP1-Responding Neurons in the VMH Are Sufficient for Sexual Behavior Enhancement

(A) Representative coronal sections from catFISH analysis in the VMHd. The stimulation conditions are shown in each image (e.g., "ESP1-none" means first: ESP1, second: no stimulus). Insets show high-magnification images of the two boxed areas in each panel. D, dorsal, L, lateral. Blue color represents DAPI nuclear staining. Scale bar, 100 μm.

(B) Proportion of dual-positive cells among nuclear *Nr4a1*+ cells (A-index). The following conditions were pooled: control, no snakeskin and control Tris buffer-ESP1; same, snakeskin-snakeskin and ESP1-ESP1; and different, snakeskin-ESP1 and ESP1-snakeskin. Error bars, SEM. The number of animals for each condition is indicated at the bottom.

(C) Schematic of the experimental setup and timeline of procedures for pharmaco-genetic activation. *AAV-FLEx-hM3Dq* was injected bilaterally into the VMHd of *Arc-CreER* female mice. CNO or saline control was intraperitoneally injected 1.5 hr before the mating assay.

(D) Lordosis percentage following i.p. injection of saline or CNO. ESP1 and snakeskin TRAP, n = 6. Basal activity TRAP, n = 3.

(E) Correlation between the activation of ESP1-responding neurons (x axis) and lordosis percentage in CNO i.p. conditions (y axis). We noticed a considerable positive correlation (R^2 = 0.39, p = 0.06), suggesting that efficient activation of the VMHd ESP1-responding neurons tended to enhance lordosis.

(F) Schematic of the experimental setup and time line of procedures for optogenetic activation. ESP1 and snakeskin TRAP animals were light stimulated for 5 min, 1 hr before the mating assay (20 Hz, 20 ms, 40% duty cycle).

(G) Lordosis percentage for light OFF or ON trials. n = 5 each.

Gray lines indicate trials from individual animals. Error bars, SEM. (B) One-way ANOVA with Bonferroni correction. a versus b, a versus c, b versus c, $p < 0.01$. (D and G) Paired Student's t test with Bonferroni correction, *$p < 0.05$. n.s., not significant. See also Figures S5 and S6.

projectors and MPA projectors with pan-*SF1* labeling without prior selection of the target as a control (Figure S7). Quantification of the axonal projections in 11 diverse brain regions revealed that the axonal arborization patterns of the *SF1*+ PAGd-projectors and MPA-projectors closely resembled those of pan-SF1 labeling (Figures S7E–S7G). Thus, in contrast to *vGluT2*+ MeApv neurons, the output structure of *SF1*+ VMHd neurons was highly divergent.

We next conducted pathway-selective inhibition of *SF1*+ neurons by utilizing hM4Di-neurexin, an axon-enriched variant of hM4Di (Stachniak et al., 2014). An AAV expressing hM4Di-neurexin in a Cre-dependent manner (*AAV-FLEx-hM4Di-neurexin*) was injected into the VMHd of *SF1-Cre* female mice. CNO was locally injected through a cannula placed above the PAGd or MPA to selectively inhibit neurotransmitter release from nearby axon terminals of *SF1*+ neurons without affecting the activities of their cell bodies or distant axon collaterals (Figures 8A, 8B, and S8). Local CNO injection into the PAGd suppressed the enhancement of lordosis mediated by ESP1, similar to i.p. injection of CNO (Figure 8C). In contrast, local CNO injection into the MPA resulted in a high percentage of lordosis, similar to saline injection (Figure 8D). Thus, we conclude that ESP1 information

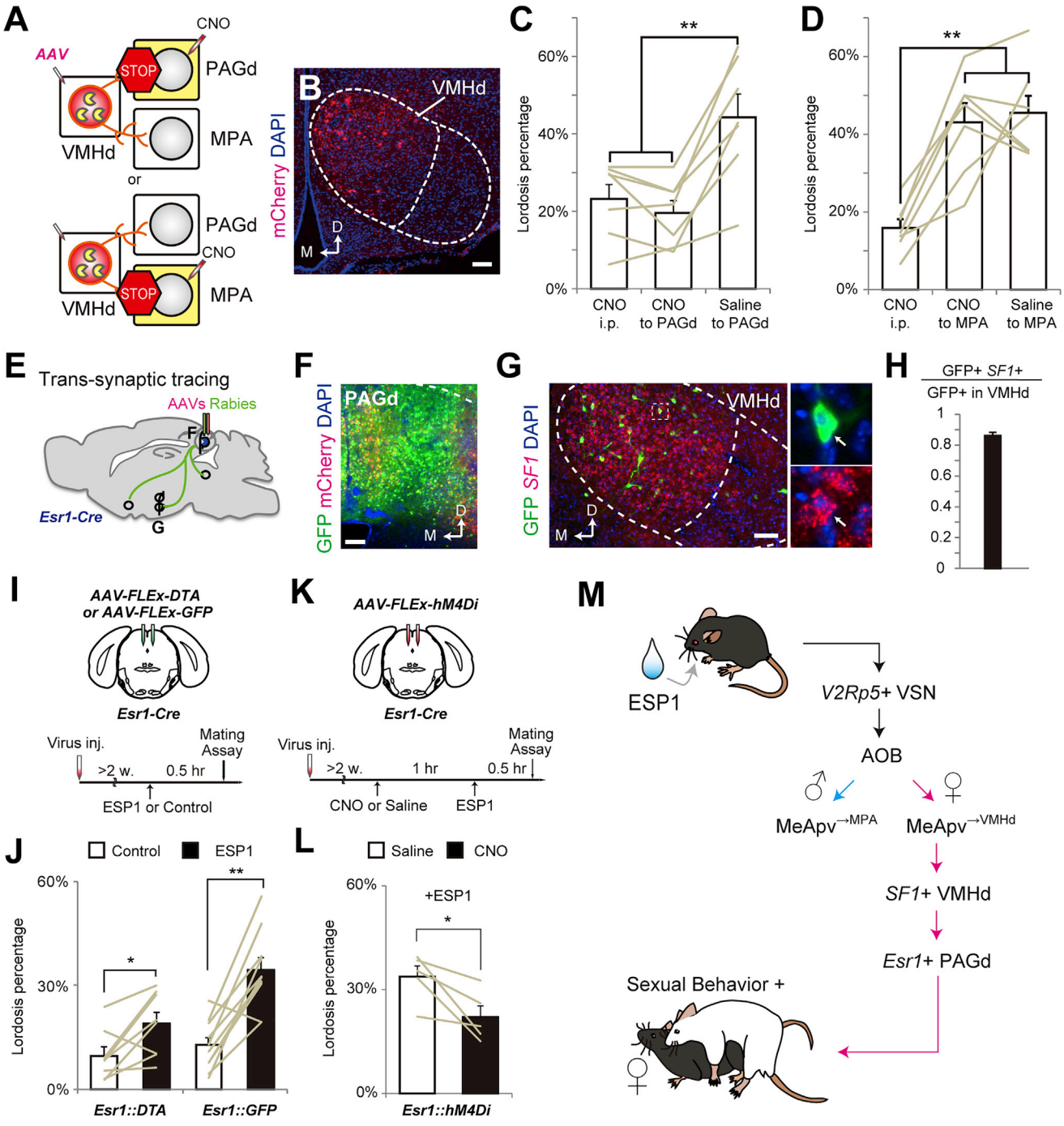

Figure 8. The *SF1*+ VMHd Neurons → *Esr1*+ PAG Neurons Pathway Is Necessary for ESP1-Mediated Enhanced Lordosis

(A) Schematic of the experimental setup for pathway selective inhibition of *SF1*+ neurons. *AAV-FLEx-hM4Di-neurexin* was injected into the VMHd of *SF1-Cre* female mice. CNO or saline was locally injected into the PAGd or MPA (see also Figure S8).

(B) A representative coronal section showing hM4Di-neurexin expression (mCherry+ shown in red) in the VMHd.

(C and D) Lordosis percentage in mice in which the PAGd pathway (C) or MPA pathway was inhibited (D). n = 7 each. One-way repeated ANOVA with Bonferroni correction.

(E) Schematic of the experimental setup for retrograde transsynaptic tracing. A blue Pac-Man symbol represents Cre expression in *Esr1-Cre* mice.

(F) A representative coronal section showing starter cells (in yellow) and local GFP labeling in the PAGd. M, medial; D, dorsal.

(G) A representative coronal section of the VMH showing GFP+ neurons (green) and *SF1* mRNA (red) expression. Right images show an example of a dual-positive GFP+ and *SF1*+ cell (arrow). We detected 111 ± 7.5 starter cells in the PAGd, which labeled 144 ± 15 GFP+ cells in the VMH (every fourth section was counted, n = 3 animals).

(legend continued on next page)

conveyed to the PAGd from *SF1*+ VMHd neurons is necessary for enhancement of lordosis. Interestingly, although *SF1*+ neurons project their axonal arbors to both the PAGd and MPA, only the PAGd pathway was necessary for enhanced lordosis, suggesting that ESP1 information is processed differently within the PAGd and MPA.

Esr1+ Neurons in the PAGd Contribute to Enhancement of Lordosis by ESP1

Previous studies have indicated that the PAG is an important area for modulation of lordosis (Sakuma and Pfaff, 1979), presumably by sensing the sex hormone estrogen (Floody et al., 1986). Therefore, we focused on *Esr1*+ PAG neurons as a candidate neural population that receives information directly from *SF1*+ VMHd neurons. To test this model, we performed rabies-mediated transsynaptic tracing (Miyamichi et al., 2013) from *Esr1*+ PAGd neurons, which allows visualization of their presynaptic neurons with GFP (Figures 8E and 8F). We observed presynaptic neurons in broad brain regions including *SF1*+ VMHd neurons, indicating monosynaptic connections from *SF1*+ VMHd neurons to *Esr1*+ PAGd neurons (Figures 8G and 8H).

We next conducted a series of loss-of-function experiments in *Esr1*+ PAGd neurons. First, we injected *AAV-FLEx-DTA* into the PAGd of *Esr1-Cre* female mice to ablate these neurons (Figure 8I). This treatment reduced ESP1-mediated enhancement of lordosis but did not affect basal lordosis (Figure 8J). These data resembled ablation of *SF1*+ neurons (Figure 6F), although the phenotype was weaker than *SF1*+ loss-of-function cases. Next, we injected *AAV-FLEx-hM4Di* into the PAGd of *Esr1-Cre* mice to inhibit neural activities of *Esr1*+ PAGd neurons by i.p. injection of CNO (Figure 8K). This treatment significantly reduced the percentage of lordosis in ESP1-exposed mice (Figure 8L), although the reduction was not as strong as inhibition of *SF1*+ neurons (Figure 6J). Together, our data demonstrated that *Esr1*+ PAGd neurons are anatomically downstream of *SF1*+ VMHd neurons and constitute a part of the system that facilitates lordosis by ESP1.

DISCUSSION

How a single sensory input robustly affects a specific behavioral output is a long-standing question, especially in mammals. Our study delineates the neural circuit responsible for enhancing sexual behavior of female mice by a single pheromone (Figure 8M). Specifically, we propose two information-sorting mechanisms in the amygdala-hypothalamus axis for pheromone-mediated behaviors in mice. The first mechanism acts at the level of brain regions: two distinct types of projection neurons with selective axonal arborization patterns in the MeApv bifurcate the information flow of the sex pheromone ESP1 to the MPA in male mice and the VMHd in female mice. This sexually dimorphic information sorting may provide the basis for the different functions of ESP1 in males and females. However, this mechanism alone cannot distinguish ESP1 signals from natural predator cues in female mice, as both signals are conveyed via the VMHd pathway. The second mechanism acts at the level of neural populations: in the MeApv and VMHd, ESP1 and snakeskin signals are conveyed by mostly distinct neural populations. These mechanisms suggest the presence of labeled-line organizations to evoke distinct behaviors by different sensory cues. Here, we discuss these two mechanisms and the novel insight provided by our study regarding how the female brain controls sexual behaviors.

Sexually Dimorphic Information Sorting in the Medial Amygdala

To send a signal to a downstream area in a sexually dimorphic manner, two extreme strategies can be envisioned: (1) the output structures differ or (2) the activation patterns of a common output structure differ between males and females. A previous study has shown a sexually dimorphic difference in the axonal density of aromatase-expressing subpopulations of neurons in the MeApd that project to the VMHvl (Wu et al., 2009), supporting the first strategy. In contrast, our study showed that the overall output structure of *vGluT2*+ MeApv neurons was sexually monomorphic and that the activation patterns by ESP1 differed drastically between the sexes (Figure 3G), providing an example of the second strategy.

Such sexually dimorphic processing of an olfactory input was also proposed for the *Drosophila* male pheromone 11-*cis*-vaccenyl acetate (cVA). Similar to ESP1 in mice, cVA enhances male aggression and female sexual behaviors in flies (Kurtovic et al., 2007; Wang and Anderson, 2010). Different third-order neurons in the lateral horn, a structure analogous to the vertebrate amygdala, respond to cVA in males and females (Kohl et al., 2013). Thus, the sexually dimorphic usage of different types of amygdala/lateral horn neurons seems to be a universal strategy to control male pheromone-mediated behaviors. In flies, activation of distinct lateral horn neurons by cVA is achieved by the sexually dimorphic connectivity between the second- and third-order neurons formed under the influence of the male-specific form of *fruitless* (Kohl et al., 2013). In contrast, the neural mechanism for sexually dimorphic sorting of ESP1 information in the MeApv of mice is not clear and will be an important topic

(H) Fraction of SF1+ neurons among GFP+ neurons in the VMHd (n = 3 animals).
(I) Schematic of the experimental setup and time line of procedures for *Esr1*+ PAGd ablation. *AAV-FLEx-DTA* or *AAV-FLEx-GFP* was injected into the PAGd of female *Esr1-Cre* mice.
(J) Lordosis percentage of *Esr1::DTA* and *Esr1::GFP* mice exposed to ESP1 or a control stimulus. Paired Student's t test. *Esr1::GFP*, n = 10 animals, *Esr1::DTA*, n = 8.
(K) Schematic of the experimental setup and time line for procedures for *Esr1*+ PAGd inhibition. *AAV-FLEx-hM4Di* was injected into the PAGd of female *Esr1-Cre* mice.
(L) Lordosis percentage following i.p. injection of saline (white) or CNO (black). n = 5 animals. Paired Student's t test.
(M) Schematic summary of the neural circuit responsible for ESP1-mediated behaviors in mice.
Error bars, SEM. Gray lines indicate trials from individual animals. *$p < 0.05$, **$p < 0.01$. Scale bars, 100 μm. See also Figures S7 and S8.

for future studies. For example, we noticed a small difference in the induction of *cFos*+ cells in the MeApd between sexes (Figure 3B), which may affect ESP1 information processing of MeApv differently by using GABAergic inter-MeA microcircuits (Bian et al., 2008). To comprehend how the MeA processes ESP1 information in a sex-dependent manner, the entire MeA microcircuit should be taken into account.

Labeled-Line Organization of the Vomeronasal System

Using an activity-dependent labeling method, we showed that the ESP1-responding subpopulation of neurons in the VMHd, which is downstream of the MeApv, is sufficient for sexual behavior enhancement in female mice. The robust enhancement of lordosis by pharmaco- or optogenetic activation of ESP1-TRAP neurons was rather surprising, given the fact that our TRAP method only captured a small proportion of actual ESP1-responding neurons (27% ± 3% of ESP1-TRAP neurons became *cFos*+ after ESP1 exposure; Figure S6C). Animals seem to be able to efficiently decode the "fragmented" neural code to evoke an appropriate behavioral response. Similar observations were previously reported by using an analogous genetic tool (Denny et al., 2014; Ye et al., 2016). This limited efficiency of the TRAP method, however, is a major obstacle to full characterization of the heterogeneity of VMHd neurons, and thus, we have to await molecular and physiological investigations of VMHd subpopulations.

Nevertheless, these behavioral data, together with histological data from catFISH analysis, indicate that in female mice, ESP1 and snakeskin signals are represented by mostly distinct neural populations in the VMHd. Furthermore, data from catFISH analysis imply that the two signals are also distinctly represented in the AOB and MeApv. Because ESP1 and snakeskin signals are received by distinct sets of receptors (Haga et al., 2010; Isogai et al., 2011), information about a sex pheromone and predator cues seems to be conveyed by a labeled-line neural circuit from the periphery sensory organ to, at least, the hypothalamus. Previous studies using sex-related or predator-related olfactory stimuli have shown that amygdala neurons tend to be tuned to a specific stimulus (Bergan et al., 2014). Together with these studies, we propose that labeled-line organization is a universal strategy to process olfactory input to evoke innately defined behavioral output.

ESP1 Delineates a Novel Lordosis-Promoting Neural Circuit in Female Mice

The VMHvl is considered a crucial center in regulating female sexual behavior in mice (Pfaff and Sakuma, 1979; Yang et al., 2013). Thus, we initially speculated that pheromones such as ESP1 that enhance sexual behaviors in female mice would activate the VMHvl. Contrary to this prediction, we found that *SF1*+ VMHd neurons and the activities of the *SF1*+ neurons → PAGd pathway were necessary for ESP1-mediated enhanced lordosis behavior, demonstrating a previously unacknowledged pathway as an important modulator of female sexual behaviors.

VMHd and VMHvl neurons seem to play different roles in sexual behaviors of female mice. Genetic ablation or inhibition of VMHd neurons only impaired enhancement of lordosis without affecting basal lordosis, whereas ablation of VMHvl neurons completely abolished basal lordosis. This observation provides a model in which the VMHvl acts as an on/off switch for basal lordosis behavior, and the VMHd provides control of the intensity of sexual receptivity. In addition to the VMHd → PAGd pathway that we analyzed in this study, the VMHvl → PAG pathway has also been proposed to promote lordosis (Pfaff et al., 2008). Signals from the VMHd and VMHvl may converge within the PAG. Further studies should reveal how the signals from these two areas interact or converge to determine the final lordosis output. The entire framework of the neural basis underlying the control of female sexual behaviors will provide a basis for understanding the central origin of sexual dysfunctions.

In conclusion, our study delineates a neural circuit for controlling sexual behaviors in female mice that was not revealed by previous brain region-based dissection. The present study describes the cell-type-specific neural basis of how a sex pheromone input is differently processed from a predator cue and converted to a specific behavioral output in female mice. This could not have been achieved without using a single purified pheromone and a corresponding receptor to evoke robust behavioral output, demonstrating the power of naturally evolved pheromones as probes to dissect neural circuits. We expect that similar approaches can be applied broadly to anatomically and functionally dissect neural circuits that mediate instinctive behaviors evoked by various chemosensory inputs in mice.

STAR★METHODS

Detailed methods are provided in the online version of this paper and include the following:

- KEY RESOURCES TABLE
- CONTACT FOR REAGENT AND RESOURCE SHARING
- EXPERIMENTAL MODEL AND SUBJECT DETAILS
  - Animals
- METHOD DETAILS
  - Generation of V2Rp5-Cre transgenic mice
  - Stereotactic injection
  - Pharmacogenetics
  - Optogenetic
  - Mating Assay and Lordosis Quantification
  - Viral Preparations
  - H129-ΔTK-TT preparation
  - Anterograde tracing with H129-ΔTK-TT
  - Axon-initiated Circuit Mapping
  - Production of Recombinant ESP1
  - Histochemistry
  - cFos Mapping and catFISH
  - TRAP
  - Rabies *Trans*-synaptic Tracing
  - Cell count
  - Schematic images
- QUANTIFICATION AND STATISTICAL ANALYSIS

SUPPLEMENTAL INFORMATION

Supplemental Information includes eight figures and one table and can be found with this article online at http://dx.doi.org/10.1016/j.neuron.2017.05.038.

AUTHOR CONTRIBUTIONS

K.T. supervised the project. K.K.I., T.O., K.M., and K.T. designed the study. K.K.I. performed the ESP1-mediated behavioral studies with manipulations of defined neurons with help from H.M., the Retrobeads experiments, and most of the data analysis. T.O. generated BAC transgenic mice and performed anterograde tracing. K.M. established viral injections and performed cFos mapping, catFISH, axon mapping, and retrograde tracing with help from H.M. Y.Y. generated *AAV-FLEx-DTA* virus and helped in the generation of the BAC transgenic mice with N.M. K.K.I. and K.M. wrote the paper with substantial contributions from T.O. and K.T.

ACKNOWLEDGMENTS

We thank L. Luo for sharing *CAV2-FLEx-Flp*, *AAV-hSyp-FLEx^{FRT}-mGFP*, and *Arc-CreER* mice; S. Sternson for sharing *AAV-CMV-FLEx-mCherry-2a-hM4Dnrxn* for pilot experiments; D.J. Anderson for sharing HSV-H129 *ΔTK-TT*; the Japan Snake Center for providing the snakeskin; E. Callaway for sharing B7GG, BHK-EnvA, and HEK293-TVA800 cell lines; K. Murata and S. Fujisawa for technical advice on optogenetics; M. Yamaguchi for sharing rabies virus; and members of the Touhara lab for their help. K.K.I. and T.O. are supported by research fellowship for young scientist from JSPS. K.T. is supported by the ERATO Touhara Chemosensory Signal Project (JST ERATO grant number JPMJER1202), and K.M. is supported by JSPS Kakenhi grant 16K20963.

Received: September 22, 2016
Revised: April 14, 2017
Accepted: May 26, 2017
Published: June 22, 2017

REFERENCES

Armbruster, B.N., Li, X., Pausch, M.H., Herlitze, S., and Roth, B.L. (2007). Evolving the lock to fit the key to create a family of G protein-coupled receptors potently activated by an inert ligand. Proc. Natl. Acad. Sci. USA *104*, 5163–5168.

Beier, K.T., Steinberg, E.E., DeLoach, K.E., Xie, S., Miyamichi, K., Schwarz, L., Gao, X.J., Kremer, E.J., Malenka, R.C., and Luo, L. (2015). Circuit architecture of VTA dopamine neurons revealed by systematic input-output mapping. Cell *162*, 622–634.

Bergan, J.F., Ben-Shaul, Y., and Dulac, C. (2014). Sex-specific processing of social cues in the medial amygdala. eLife *3*, e02743.

Bian, X., Yanagawa, Y., Chen, W.R., and Luo, M. (2008). Cortical-like functional organization of the pheromone-processing circuits in the medial amygdala. J. Neurophysiol. *99*, 77–86.

Boyden, E.S., Zhang, F., Bamberg, E., Nagel, G., and Deisseroth, K. (2005). Millisecond-timescale, genetically targeted optical control of neural activity. Nat. Neurosci. *8*, 1263–1268.

Canteras, N.S. (2002). The medial hypothalamic defensive system: hodological organization and functional implications. Pharmacol. Biochem. Behav. *71*, 481–491.

Choi, G.B., Dong, H.W., Murphy, A.J., Valenzuela, D.M., Yancopoulos, G.D., Swanson, L.W., and Anderson, D.J. (2005). Lhx6 delineates a pathway mediating innate reproductive behaviors from the amygdala to the hypothalamus. Neuron *46*, 647–660.

Denny, C.A., Kheirbek, M.A., Alba, E.L., Tanaka, K.F., Brachman, R.A., Laughman, K.B., Tomm, N.K., Turi, G.F., Losonczy, A., and Hen, R. (2014). Hippocampal memory traces are differentially modulated by experience, time, and adult neurogenesis. Neuron *83*, 189–201.

Dhillon, H., Zigman, J.M., Ye, C., Lee, C.E., McGovern, R.A., Tang, V., Kenny, C.D., Christiansen, L.M., White, R.D., Edelstein, E.A., et al. (2006). Leptin directly activates SF1 neurons in the VMH, and this action by leptin is required for normal body-weight homeostasis. Neuron *49*, 191–203.

Dulac, C., and Wagner, S. (2006). Genetic analysis of brain circuits underlying pheromone signaling. Annu. Rev. Genet. *40*, 449–467.

Floody, O.R., Lisk, R.D., and Vomachka, A.J. (1986). Facilitation of lordosis by estradiol in the mesencephalic central gray. Physiol. Behav. *37*, 587–595.

Franklin, K.B.J., and Paxinos, G. (2007). The Mouse Brain in Stereotaxic Coordinates (Academic Press).

Guenthner, C.J., Miyamichi, K., Yang, H.H., Heller, H.C., and Luo, L. (2013). Permanent genetic access to transiently active neurons via TRAP: targeted recombination in active populations. Neuron *78*, 773–784.

Guzowski, J.F., McNaughton, B.L., Barnes, C.A., and Worley, P.F. (1999). Environment-specific expression of the immediate-early gene Arc in hippocampal neuronal ensembles. Nat. Neurosci. *2*, 1120–1124.

Haga, S., Hattori, T., Sato, T., Sato, K., Matsuda, S., Kobayakawa, R., Sakano, H., Yoshihara, Y., Kikusui, T., and Touhara, K. (2010). The male mouse pheromone ESP1 enhances female sexual receptive behaviour through a specific vomeronasal receptor. Nature *466*, 118–122.

Hattori, T., Osakada, T., Matsumoto, A., Matsuo, N., Haga-Yamanaka, S., Nishida, T., Mori, Y., Mogi, K., Touhara, K., and Kikusui, T. (2016). Self-exposure to the male pheromone ESP1 enhances male aggressiveness in mice. Curr. Biol. *26*, 1229–1234.

Ikeda, Y., Luo, X., Abbud, R., Nilson, J.H., and Parker, K.L. (1995). The nuclear receptor steroidogenic factor 1 is essential for the formation of the ventromedial hypothalamic nucleus. Mol. Endocrinol. *9*, 478–486.

Isogai, Y., Si, S., Pont-Lezica, L., Tan, T., Kapoor, V., Murthy, V.N., and Dulac, C. (2011). Molecular organization of vomeronasal chemoreception. Nature *478*, 241–245.

Kimoto, H., Haga, S., Sato, K., and Touhara, K. (2005). Sex-specific peptides from exocrine glands stimulate mouse vomeronasal sensory neurons. Nature *437*, 898–901.

Kohl, J., Ostrovsky, A.D., Frechter, S., and Jefferis, G.S.X.E. (2013). A bidirectional circuit switch reroutes pheromone signals in male and female brains. Cell *155*, 1610–1623.

Kunwar, P.S., Zelikowsky, M., Remedios, R., Cai, H., Yilmaz, M., Meister, M., and Anderson, D.J. (2015). Ventromedial hypothalamic neurons control a defensive emotion state. eLife *4*, e06633.

Kurtovic, A., Widmer, A., and Dickson, B.J. (2007). A single class of olfactory neurons mediates behavioural responses to a Drosophila sex pheromone. Nature *446*, 542–546.

Lee, H., Kim, D.-W., Remedios, R., Anthony, T.E., Chang, A., Madisen, L., Zeng, H., and Anderson, D.J. (2014). Scalable control of mounting and attack by Esr1+ neurons in the ventromedial hypothalamus. Nature *509*, 627–632.

Lin, D., Boyle, M.P., Dollar, P., Lee, H., Lein, E.S., Perona, P., and Anderson, D.J. (2011). Functional identification of an aggression locus in the mouse hypothalamus. Nature *470*, 221–226.

Lindberg, D., Chen, P., and Li, C. (2013). Conditional viral tracing reveals that steroidogenic factor 1-positive neurons of the dorsomedial subdivision of the ventromedial hypothalamus project to autonomic centers of the hypothalamus and hindbrain. J. Comp. Neurol. *521*, 3167–3190.

Lo, L., and Anderson, D.J. (2011). A Cre-dependent, anterograde transsynaptic viral tracer for mapping output pathways of genetically marked neurons. Neuron *72*, 938–950.

Lonstein, J.S., and Gammie, S.C. (2002). Sensory, hormonal, and neural control of maternal aggression in laboratory rodents. Neurosci. Biobehav. Rev. *26*, 869–888.

Maxwell, M.A., and Muscat, G.E. (2006). The NR4A subgroup: immediate early response genes with pleiotropic physiological roles. Nucl. Recept. Signal. *4*, e002.

Miyamichi, K., Shlomai-Fuchs, Y., Shu, M., Weissbourd, B.C., Luo, L., and Mizrahi, A. (2013). Dissecting local circuits: parvalbumin interneurons underlie broad feedback control of olfactory bulb output. Neuron *80*, 1232–1245.

Newman, S.W. (1999). The medial extended amygdala in male reproductive behavior. A node in the mammalian social behavior network. Ann. N Y Acad. Sci. *877*, 242–257.

Osakada, F., and Callaway, E.M. (2013). Design and generation of recombinant rabies virus vectors. Nat. Protoc. *8*, 1583–1601.

Papes, F., Logan, D.W., and Stowers, L. (2010). The vomeronasal organ mediates interspecies defensive behaviors through detection of protein pheromone homologs. Cell *141*, 692–703.

Pfaff, D.W., and Sakuma, Y. (1979). Deficit in the lordosis reflex of female rats caused by lesions in the ventromedial nucleus of the hypothalamus. J. Physiol. *288*, 203–210.

Pfaff, D.W., Kow, L.M., Loose, M.D., and Flanagan-Cato, L.M. (2008). Reverse engineering the lordosis behavior circuit. Horm. Behav. *54*, 347–354.

Sakuma, Y., and Pfaff, D.W. (1979). Mesencephalic mechanisms for integration of female reproductive behavior in the rat. Am. J. Physiol. *237*, R285–R290.

Schwarz, L.A., Miyamichi, K., Gao, X.J., Beier, K.T., Weissbourd, B., DeLoach, K.E., Ren, J., Ibanes, S., Malenka, R.C., Kremer, E.J., and Luo, L. (2015). Viral-genetic tracing of the input-output organization of a central noradrenaline circuit. Nature *524*, 88–92.

Silva, B.A., Mattucci, C., Krzywkowski, P., Murana, E., Illarionova, A., Grinevich, V., Canteras, N.S., Ragozzino, D., and Gross, C.T. (2013). Independent hypothalamic circuits for social and predator fear. Nat. Neurosci. *16*, 1731–1733.

Stachniak, T.J., Ghosh, A., and Sternson, S.M. (2014). Chemogenetic synaptic silencing of neural circuits localizes a hypothalamus→midbrain pathway for feeding behavior. Neuron *82*, 797–808.

Touhara, K., and Vosshall, L.B. (2009). Sensing odorants and pheromones with chemosensory receptors. Annu. Rev. Physiol. *71*, 307–332.

Tsuneoka, Y., Tokita, K., Yoshihara, C., Amano, T., Esposito, G., Huang, A.J., Yu, L.M.Y., Odaka, Y., Shinozuka, K., McHugh, T.J., and Kuroda, K.O. (2015). Distinct preoptic-BST nuclei dissociate paternal and infanticidal behavior in mice. EMBO J. *34*, 2652–2670.

Vong, L., Ye, C., Yang, Z., Choi, B., Chua, S., Jr., and Lowell, B.B. (2011). Leptin action on GABAergic neurons prevents obesity and reduces inhibitory tone to POMC neurons. Neuron *71*, 142–154.

Wang, L., and Anderson, D.J. (2010). Identification of an aggression-promoting pheromone and its receptor neurons in Drosophila. Nature *463*, 227–231.

Wang, L., Chen, I.Z., and Lin, D. (2015). Collateral pathways from the ventromedial hypothalamus mediate defensive behaviors. Neuron *85*, 1344–1358.

Wu, M.V., Manoli, D.S., Fraser, E.J., Coats, J.K., Tollkuhn, J., Honda, S., Harada, N., and Shah, N.M. (2009). Estrogen masculinizes neural pathways and sex-specific behaviors. Cell *139*, 61–72.

Wu, Z., Autry, A.E., Bergan, J.F., Watabe-Uchida, M., and Dulac, C.G. (2014). Galanin neurons in the medial preoptic area govern parental behaviour. Nature *509*, 325–330.

Xiu, J., Zhang, Q., Zhou, T., Zhou, T.T., Chen, Y., and Hu, H. (2014). Visualizing an emotional valence map in the limbic forebrain by TAI-FISH. Nat. Neurosci. *17*, 1552–1559.

Yagi, T., Ikawa, Y., Yoshida, K., Shigetani, Y., Takeda, N., Mabuchi, I., Yamamoto, T., and Aizawa, S. (1990). Homologous recombination at c-fyn locus of mouse embryonic stem cells with use of diphtheria toxin A-fragment gene in negative selection. Proc. Natl. Acad. Sci. USA *87*, 9918–9922.

Yang, C.F., Chiang, M.C., Gray, D.C., Prabhakaran, M., Alvarado, M., Juntti, S.A., Unger, E.K., Wells, J.A., and Shah, N.M. (2013). Sexually dimorphic neurons in the ventromedial hypothalamus govern mating in both sexes and aggression in males. Cell *153*, 896–909.

Ye, L., Allen, W.E., Thompson, K.R., Tian, Q., Hsueh, B., Ramakrishnan, C., Wang, A.-C., Jennings, J.H., Adhikari, A., Halpern, C.H., et al. (2016). Wiring and molecular features of prefrontal ensembles representing distinct experiences. Cell *165*, 1776–1788.

STAR★METHODS

KEY RESOURCES TABLE

REAGENT or RESOURCE	SOURCE	IDENTIFIER
Antibodies		
horseradish peroxidase (HRP) conjugated anti-Dig antibody	Roche Applied Science	cat#11207733910
horseradish peroxidase (HRP) conjugated anti-Flu antibody	PerkinElmer	cat#NEF710001EA
goat anti-cFos antibody	Santa Cruz Biotechnology	cat#sc-52-g
rat anti-mCherry antibody	Life Technology	cat#M11217
donkey anti-rat IgG, Cy3 conjugated	Millipore	cat#AP189C
goat anti-chicken IgY, Alexa Fluor 488	Invitrogen	cat#A11039
donkey anti-goat IgG, Alexa Fluor 488	Invitrogen	cat#A11055
chicken anti-GFP antibody	Aves Labs	cat#GFP-1020
Bacterial and Virus Strains		
AAV serotype 8 *hSyn-GFP-Cre*	UNC Vector Core	Lot#AV5053b
AAV serotype 8 *hSyn-DIO-eGFP*	UNC Vector Core	Lot#AV4937b
AAV serotype 8 *hSyn-DIO-hM4D(Gi)-mCherry*	UNC Vector Core	Lot#AV4980F, Lot#AV4980a
AAV serotype 8 *hSyn-DIO-hM3D(Gq)-mCherry*	UNC Vector Core	Lot#AV4979h
AAV serotype 5 *EF1a-DIO-hChR2(H134R)-EYFP*	UNC Vector Core	Lot#AV4313s
AAV serotype 9 *hSyn-FLEx(FRT)-mGFP-2a-SypRuby*	Beier et al., 2015 (Custom made by UNC Vector Core)	N/A
AAV serotype 9 *CMV-FLEx-mCherry-2a-hM4Dnrxn*	Stachniak et al., 2014 (Custom made by UNC Vector Core)	N/A
AAV serotype 2 *CAG-FLEx-TCb*	Miyamichi et al., 2013 (Custom made by UNC Vector Core)	N/A
AAV serotype 2 *CAG-FLEx-RG*	Miyamichi et al., 2013 (Custom made by UNC Vector Core)	N/A
CAV2-FLEx-Flp	Schwarz et al., 2015 (Plateforme de Vectorologie de Montpellier)	N/A
AAV serotype 5 *CAG-FLEx-DTA*	This paper (Custom made by UNC Vector Core)	N/A
H129-ΔTK-TT	Amplified in the lab from a virus shared by Dr. David J. Anderson	Lo and Anderson, 2011
Rabies *dG-GFP*+EnvA	Amplified in the lab from a virus shared by Dr. Masahiro Yamaguchi	Osakada and Callaway, 2013
Biological Samples		
Elaphe climacophora shedding	Japan Snake Center	N/A
Chemicals, Peptides, and Recombinant Proteins		
streptavidin-Alexa Fluor 488	Life Technologies	cat#S32354
red Retrobeads	Lumafluor	N/A
TSA-plus Cyanine 3	PerkinElmer	cat#NEL744001KT
TSA-plus biotin	PerkinElmer	cat#NEL749A001KT
Experimental Models: Cell Lines		
B7GG cell line	Gift from Dr. Edward Callaway	Osakada and Callaway, 2013
BHK-EnvA cell line	Gift from Dr. Edward Callaway	Osakada and Callaway, 2013
HEK293-TVA800 cell line	Gift from Dr. Edward Callaway	Osakada and Callaway, 2013
Experimental Models: Organisms/Strains		
Mouse: SF1-Cre (Tg(Nr5a1-cre)7Lowl)	JAX Laboratories	Jax#012462
Mouse: vGluT2-Cre (B6J.129S6(FVB)-Slc17a6$^{tm2(cre)Lowl}$/MwarJ)	JAX Laboratories	Jax#028863

(*Continued on next page*)

Continued

REAGENT or RESOURCE	SOURCE	IDENTIFIER
Mouse: Esr1-Cre (B6N.129S6(Cg)-Esr1$^{tm1.1(cre)And}$/J)	JAX Laboratories	Jax#017911
Mouse: Arc-CreER (B6.129(Cg)-Arc$^{tm1.1(cre/ERT2)Luo}$/J)	Gift from Dr. Liqun Luo	Jax#021881
Oligonucleotides		
Primers for RNA probes, see **Table S1**	This paper (Custom made by Hokkaido System Science Co.)	N/A
Recombinant DNA		
Plasmid: *pAAV hSyn FLExFRT mGFP-2A-Synaptophysin-mRub*	Beier et al., 2015	Addgene Plasmid #71761
Plasmid: *AA0250-mCherry-2a-hM4D-nrxn1a rev*	Stachniak et al., 2014	Addgene Plasmid #60544
Plasmid: *CAG-FLEX-TCB*	Miyamichi et al., 2013	Addgene Plasmid #48332
Plasmid: *CAG-FLEX-RG*	Miyamichi et al., 2013	Addgene Plasmid #48333
mouse whole brain cDNA	GenoStaff	cat#MD01

CONTACT FOR REAGENT AND RESOURCE SHARING

Further information and requests for resources and reagents should be directed to and will be fulfilled by the Lead Contact, Kazushige Touhara (ktouhara@mail.ecc.u-tokyo.ac.jp).

EXPERIMENTAL MODEL AND SUBJECT DETAILS

Animals

Animals were housed under a regular 12 hr dark/light cycle with food and water ad libitum. Wild-type ICR mice were purchased from Japan CLEA (Tokyo, Japan). Wild-type C57BL/6 mice were purchased from Japan CLEA for histological experiments and from Japan SLC (Shizuoka, Japan) for behavioral experiments. *SF1-Cre* (also known as *Nr5a1-Cre*, Jax#012462), *vGluT2-Cre* (also known as *Slc17a6-ires-Cre*, Jax#028863), and *Esr1-Cre* (Jax#017911) mice were purchased from the Jackson laboratory. *Arc-CreER* (Jax#021881) mice were provided by Dr. Luo (Stanford University). All male mice which were used as intruders were singly housed to avoid male-male aggression. Female mice with optic fibers or cannulas were singly housed. All other mice were group housed. All animal procedures followed animal care guidelines approved by the University of Tokyo.

METHOD DETAILS

Experimental protocols involving rabies virus, canine adenovirus type 2 (CAV2), and herpes simplex virus type 1 (HSV1) followed Biosafety Level 2 (P2/P2A) procedures approved by the biosafety committee of the Graduate School of Agricultural and Life Sciences, the University of Tokyo.

Generation of V2Rp5-Cre transgenic mice

To generate BAC transgenic lines expressing nuclear localized Cre (nCre) under the control of *V2Rp5* locus, a BAC construct was generated as described previously (Haga et al., 2010) by inserting *IRES2-nCre-Kan^r* cassette immediately downstream of the stop codon of the *V2Rp5* gene in the BAC clone RPCI-23-265G20 (Children's Hospital Oakland Research Institute, Oakland, California). *IRES2-nCre-Kan^r* targeting vector was constructed by recombinant PCR and regular cloning methods from *pCAG-GS-NCre-polyA*, *pGEM-T-Easy-Kan^r* which were custom made in the lab, and from a purchased plasmid *pIRES2-DsRed-Express2* (Clontech, cat#632540). The modified BAC construct was purified using NucleoBond BAC 100 (Machery-Nagel, cat#740579), linearized by NotI, and injected into C57BL/6 fertilized eggs to generate transgenic mice. We established and used three independent transgenic lines with comparable number of *Cre*+ cells in the VNO.

To visualize the expression patterns of *V2Rp5* and *Cre*, two-color fluorescent *in situ* hybridization (ISH) was performed (Figure 1B). Methods for generating Flu-labeled *Cre*-probes are described in Histochemistry. DIG-labeled *V2Rp5*-probe was prepared as described previously (Haga et al., 2010). First, sequences for *V2Rp5* was obtained from the VNO by 5′-RACE using the following primers: 5′-CTGGTCAGACAAGAAGTTACTTAGG-3′. The amplified DNA was subcloned into the vector *pBlueScript II SK* (+) (addgene, cat#212205). The modified vector was linearized by NotI and purified using Wizard SV Gel and PCR Clean-Up System (Promega, cat#A9281). The DNA vector template (about 1000 ng) was subject to in vitro transcription with DIG-RNA labeling mix (Roche Applied Science, cat#11277073910) and T7 RNA polymerase (Promega, cat#P2075) according to the manufacture's instruction. After DNase I treatment (Promega, cat#M6101) for 20 min at 37°C, the RNA probe was purified by Fast Gene Dye Terminator Removal Kit (NIPPON Genetics, cat#FG9411).

To collect VNO, mice were anesthetized with sodium pentobarbital and perfused. Snouts were removed and post-fixed in 4% paraformaldehyde (PFA) in PBS for 3 hr at 4°C, decalcified in 0.5 M EDTA for 48 hr at 4°C, and cryoprotected in 30% sucrose solutions in PBS at 4°C. Then, 14 μm coronal sections of the nasal cavity were collected onto MAS-coated glass slides (Matsunami Glass).

Two-color fluorescent *in situ* hybridization of VNO sections was conducted as described in (Hattori et al., 2016). *V2Rp5-Cre* mice were anesthetized with pentobarbital sodium and perfused quickly. Snouts were removed and post-fixed in 4% paraformaldehyde (PFA) in PBS for 3 hr at 4, decalcified in 0.5 M EDTA for 48 hr at 4°C and cryoprotected in 30% sucrose solutions in PBS at 4°C. Then, 14-μm coronal sections of the nasal cavity were collected onto MAS-coated glass slides (Matsunami Glass). First, the slide with VNO sections was fixed in 4% PFA in PBS for 10 min, and washed three times with PBS each for 5 min. The slide was treated with 0.1% H_2O_2 in PBS for 30 min, and after subsequent washing with PBS, treated with 2 μg/ml protease K (Thermo Fisher Scientific cat#25530049) in TE solution (10 mM Tris-Cl (pH 7.4) and 1 mM EDTA (pH 8.0)) for 5 min at 37°C. After incubation with 4% PFA for 10 min at r.t. and three washes with PBS, the slide was then treated with acetylation solution (0.1 M triethanolamine with 2.5 μl/ml acetic anhydride) for 10 min. After washing with PBS, the slide was incubated with the pre-hybridization solution (50% formamide (Sigma-Aldrich cat#F9037), 5 × SSC, 5 × Denhardt's (Life Technologies cat#750018), 2.5 mg/ml tRNA (Life Technologies cat#15401-029), 0.5 mg/ml herring sperm DNA (Promega cat#D1811)) for 2 hr at 60°C. The hybridization buffer (sodium dextran sulfate (Nacalai tesque, cat#10912-92) was added into pre-hybridization solution in the final concentration to be 4%) containing *Flu*-labeled *Cre* probes (a cocktail of three probes to cover nearly the full length of *Cre* mRNA) and DIG-labeled *V2Rp5* probe was heated at 95°C for 3 min and immediately chilled on ice for 5 min. After the post-hybridization washes, 300 μl of blocking solution (PerkinElmer, cat#FP1020, 0.5% blocking reagent in TBS) was applied and incubated for 45 min at room temperature, and then 300 μl of anti-Flu HRP conjugate (PerkinElmer, cat#NEF710001EA, at 1/250 dilution in the blocking solution) was applied and incubated for 3 hr at 28°C. The slide was washed with TBST for a total of 30 min, with buffer exchanges every 10 min. The signal was developed using the TSA biotin plus kit (PerkinElmer, cat#FP1441, at 1/50 dilution, for 15 min). The slide was washed with TBST (three times, 10 min each), and subsequently treated with 2% H_2O_2 in PBS. The slide was washed with PBS for 5 min and three times with TBST each for 5 min. DIG antibody solution (anti-DIG HRP conjugate (Roche, cat#11207733910) at 1/250 dilution, and Streptavidin-Alexa488 (Invitrogen, cat#S32354) at 1/250 dilution in the blocking solution) was applied to the slide and incubated for 18 hr at 4°C. After washing the slide with TBST (three times, 10 min each), the signal was developed using the TSA Cy3 plus kit (Perkin Elmer, cat#FP1170, at 1/50 dilution, for 12 min). The slide was washed with TBST, and mounted with Fluoromount (Diagnostic BioSystems). All the images were acquired using BX51N (Olympus).

Stereotactic injection

For targeting AAV or Retrobeads into a certain brain region, stereotactic coordinates were defined for each brain region based on the brain atlas (Franklin and Paxinos, 2007). Mice were anesthetized with 65 mg/kg ketamine (Daiichi-Sankyo) and 13 mg/kg xylazine (Sigma-Aldrich) via intra-peritoneal (I.P.) injection and head-fixed to a stereotactic equipment (Narishige). For AAV injection, 200–300 nL of AAV (for the experiments in Figure 2, mixture of AAV expressing Cre and AAV conditionally expressing an effector in a ratio of 1:10) was injected into the target brain region at a speed of 50–100 nl/min using UMP3 pump regulated by Micro-4 (World Precision Instruments). The following coordinates were used [Distance in millimeters from the Bregma for the anterior (A)-posterior (P) and lateral (L) positions, and from the brain surface for ventral (V) direction]: BNST, A 0.4, L 0.3, V 3.6; MPA, A 0.4 L 0.4, V 4.75; MeA P 1.1 L 2.1, V 4.95; PMCo P 2.9 L 2.7 V 5.3; VMHd P 1.0 L 0.25, V 5.25; VMHvl P 1.1 L 0.55 V 5.50. For dorsal PAG, we used the Lambda to define the anterior-posterior position, and A 0.3, L 0.40, V 1.70 was used. After viral injection, the incision was sutured and the animal was warmed using a heat pad to facilitate recovery from anesthesia. This allowed us to infect 5–15% of the cells in the target brain area (estimated by the number of labeled cells and total DAPI+ cells in the area). The animal was returned to the home cage and housed in a group until the beginning of the behavioral assay. For retrograde labeling of MeA neurons (Figure 3), 200-250 nL of red Retrobeads (Lumafluor) were bilaterally injected into the MPA or the VMHd at a speed of 50–100 nl/min using the coordinates noted above. Anesthesia and post-surgery steps were the same as the AAV injection protocol.

Pharmacogenetics

For neural activation or inactivation experiments using hM3Dq or hM4Di (Figures 2, 5, 6, 7, and 8), 0.2 mL of 0.1 μg/ml clozapine-N-oxide dissolved in saline (CNO, Sigma-Aldrich cat#C0832) or 0.2 mL of saline was I.P. injected into the animal 1 hr prior to the pheromone exposure and 1.5 hr prior to male entry. We confirmed that hM3Dq and hM4Di efficiently enhanced or silenced neural activity by IEG-based histological analysis (data not shown for hM3Dq, Figures 5D–5G for hM4Di). For pathway-selective inactivation using hM4Di-neurexin (Figures 8A–8D), a guide cannula (Plastics one) was placed above each target using the following coordinates: PAGd, 2.0 mm guide cannula (cat#C315GA/SPC) to the Lambda, Midline, V 0.65. MPA, 5.0 mm guide cannula (cat#C235GS-0.8/SPC) to A 3.5, L ± 0.4, V 3.7. Guide cannulas were permanently fixed to the skull using a layer of C&B Super bond (Sun Medical) followed by Unifast2 (GC Corporation). For local injection of CNO, 0.1 μg/ml CNO or saline (100 nL for PAGd or 50 nL for MPA) was injected locally into the animal at a speed of 50 nl/min through an internal cannula (Plastics one, cat#C315IA/SPC for PAGd, cat#C235IS/SPC for MPA) connected to the guide cannula by UMP3 pump regulated by Micro-4. The internal cannula was designed to target 1 mm below the tip of the guide cannula. Injection was confirmed by monitoring the liquid surface of the solution, and reconfirmed by injecting 50 nL of colored dye (green Retrobeads, dissolved in saline to 1:10 dilution) before sacrifice. Previous studies

have shown that CNO injection in this condition would spread approximately in a 1 mm diameter sphere, which will not affect cell bodies of *SF1*+ neurons in the VMHd (Stachniak et al., 2014).

Optogenetic

For neural activation using ChR2 (Figure 7), we constructed an optic-fiber cannula by inserting a 0.39-NA, 200-μm core multimode fiber (Thorlabs, cat#FT200UMT) into a 1.25-mm ferrule (Thorlabs, cat#CFLC230-10). Fiber tips were polished using Connectorization kit (Thorlabs, cat#CK03) and evaluated for light power at the fiber ending using power meter (Thorlabs). Optic-fiber cannulas were implanted following viral injection aimed 300–500 μm above VMHd using the following coordinates: P 1.0, L 0.25, V 4.95. Cannulas were permanently fixed to the skull using a layer of C&B Super bond (Sun Medical) followed by Unifast2 (GC Corporation). For light stimulation (light ON), cannulas were connected to a 473 nm laser (Changchun New Industries) through a 0.39-NA patch cord (Thorlabs, cat#RJPF2). Light (5.0 mW, 20 Hz, 20 ms pulse) was delivered for 5 min. For control (light OFF), cannulas were connected to the laser for 5 min with no light delivery.

Mating Assay and Lordosis Quantification

Mating assay was conducted as previously described (Haga et al., 2010) with modifications. Female mice older than 6 weeks were ovariectomized (OVX) under ketamine based anesthesia. If necessary, mice underwent surgeries for AAV injections, cannula implantation, and/or optic-fiber implantation on the same day. After more than 2 weeks of recovery, the OVX females were isolated and primed with 0.1 mL estrogen (Wako, 0.4 mg/ml) dissolved in corn oil (Sigma-Aldrich) at 24 and 48h before assay, and 0.05 mL progesterone (Wako, 10 mg/ml in corn oil) at 4h before assay. If necessary, mice underwent I.P. injection of CNO/saline, light mediated activation of ChR2 expressing neurons, or pheromone exposure as described in experimental setup. ICR mice (Japan SLC), which do not secrete ESP1, were used as a stud male, and were introduced to the female cage. These stud males had been trained to mount females at least 20 times in 30 min. Each assay was conducted 1–2 hr after the onset of dark period, under a red dim light and videotaped for subsequent 30 min for analysis of sexual behavior from a ventral view 10 min after the entry of a male partner. For Figures 2, 5H–5I, 6G–6K, 7C–7E, and 8I–8L, females underwent two mating assays at > 1 week interval, with different treatment (e.g., control or ESP1, saline or CNO, light OFF or ON). The order of treatment was randomized. Different stud males were used for each assay. Note that we did not observe any basal difference in lordosis behavior between 1st and 2nd assay.

For Figures 8A–8D, females underwent three assays with first CNO I.P. injection. After the first assay, mice received cannula implantation surgery, followed by approximately 2 weeks of recovery. After recovery, females underwent two more mating assays in > 1 week interval, with CNO or saline local injection, in a random order.

The total number of stud male mounts and female lordosis behavior upon mounts were counted as previously described (Haga et al., 2010). Mount was defined as a stud male using both forepaws to climb onto a female from behind for copulation. Lordosis behavior was defined as a female with all four paws grounded, the hind region elevated from the floor of the test chamber, no evidence of attempt to escape or exhibition of a defensive upright posture, and the back slightly arched. Experimenters were blind for the stimulation, drug or AAV condition during behavior annotation.

Viral Preparations

We obtained the following AAV vectors from UNC viral core. The viral titer was estimated based on the quantitative PCR and indicated as genome particles (gp) per ml.

- AAV serotype 8 *hSyn-GFP-Cre* (4.9×10^{12} gp/ml)
- AAV serotype 8 *hSyn-DIO-eGFP* (8×10^{12} gp/ml)
- AAV serotype 8 *hSyn-DIO-hM4D(Gi)-mCherry* (5.3×10^{12} gp/ml)
- AAV serotype 8 *hSyn-DIO-hM3D(Gq)-mCherry* (6.3×10^{12} gp/ml)
- AAV serotype 5 *EF1a-DIO-hChR2(H134R)-EYFP* (6.2×10^{12} gp/ml)

The following AAV vectors were generated de novo by UNC viral core using the corresponding plasmids as described in the original literatures.

- AAV serotype 9 *hSyn-FLEx(FRT)-mGFP-2a-SypRuby* (3.6×10^{12} gp/ml) (Beier et al., 2015)
- AAV serotype 9 *CMV-FLEx-mCherry-2a-hM4Dnrxn* (1.2×10^{12} gp/ml) (Stachniak et al., 2014)
- AAV serotype 2 *CAG-FLEx-TCb* (1.2×10^{13} gp/ml) (Miyamichi et al., 2013)
- AAV serotype 2 *CAG-FLEx-RG* (2.4×10^{12} gp/ml) (Miyamichi et al., 2013)

CAV2-FLExFlp (4.5×10^{12} gp/ml) (Beier et al., 2015; Schwarz et al., 2015) was purchased from Plateforme de Vectorologie de Montpellier (PVM, France).

To generate AAV5 *CAG-FLEx-DTA*, *DTA* sequence from *pMC1DT-A* (Oriental Yeast) (Yagi et al., 1990) was ligated to *pAAV-FLEX* sequence from *pAAV-FLEX-GFP* (Addgene). The AAV vector (AAV serotype 5 *CAG-FLEx-DTA*, 4.5×10^{12} gp/ml) was generated by UNC viral core using this plasmid.

The anterograde tracer H129-ΔTK-TT was kindly gifted by Dr. Anderson (Caltech). H129-ΔTK-TT (7.2×10^{10} pfu/ml, based on the plaque assay with serial dilution of the viral solution) was prepared as described in H129-ΔTK-TT Preparation.

RV*dG-GFP* was prepared as described in Rabies Trans-synaptic Tracing. The EnvA-pseudotyped RV*dG*-GFP+EnvA titer was estimated to be 1×10^9 infectious particles/ml based on serial dilutions of the virus stock followed by infection of the HEK293-TVA800 cell line.

H129-ΔTK-TT preparation

Infection of cultured Vero cells with H129-ΔTK-TT was performed in tissue culture plates. After the cells showed clear cytopathic effect, medium and cells were collected together. The medium and cells were frozen in dry ice, quickly thawed out in 37°C water bath and vortexed. These procedures were repeated three times. After the final vortex, medium containing the viruses was collected and spun down to remove their cell debris. Then, the supernatant was passed through a 0.45 μm filter (Millipore, cat#1365) and centrifuged at 24000 rpm/ 100 min in centrifuge tubes (BECKMAN COULTER, cat#326823) using Avanti HP-30I (BECKMAN COULTER). Dissolved viruses were aliquoted and stored at −80°C. The titer of stocks was determined using standard plaque assay on Vero cells and titers were expressed as plaque-forming units per milliliter. These procedures were based on the method described previously (Lo and Anderson, 2011).

Anterograde tracing with H129-ΔTK-TT

Anterograde viral tracing with H129-ΔTK-TT was performed in *V2Rp5-Cre* mice at 9–16 weeks of age. Mice were anesthetized with ketamine and xylazine via I.P. injection. H129-ΔTK-TT (250 nl) was injected into the glomerular layer of the left accessory olfactory bulb (AOB) using stereotaxic equipment (Narishige). The coordinates were 0.9 mm lateral from midline, 3.3 mm anterior from the Bregma, and 2.25 mm ventral from the surface of the brain with the mouse head inclining forward at 20 degrees. After recovery, mice were housed in biosafety level 2 (BSL2) facilities for 1–6 days before euthanasia. Brains were removed and post-fixed in 4% paraformaldehyde (PFA) in PBS for 3 hr at 4°C. Brains were cryoprotected in 15% and 30% sucrose solutions in PBS at 4°C over two nights. Forty-micron coronal sections of the brain were collected onto MAS-coated glass slides (Matsunami Glass). Snouts were decalcified in 0.5 M EDTA for 48 hr at 4°C and cryoprotected in 15% and 30% sucrose solutions in PBS at 4°C over two nights. Fourteen-micron coronal sections of the nasal cavity were collected onto MAS-coated glass slides (Matsunami Glass).

tdTomato signals of H129-ΔTK-TT were detected with fluorescent *in situ* hybridization as described in **Histochemistry**. Three to four images were taken from 40-μm coronal section (every 3rd section) in each of the five brain regions (BNST, MeA, PMCo, MPA, and VMH) with a 10x objective by using an Olympus epifluorescence microscope (BX53) equipped with ORCA-R2 cooled CCD camera (Hamamatsu Photonics).

Axon-initiated Circuit Mapping

To visualize glutamatergic VMHd- or MPA-projectors in the MeA (Figure 4), 100 nL of AAV9 *hSyp-FLEx^{FRT}-mGFP-2a-SypRuby* was injected into the MeA of heterozygous *vGluT2-Cre* mice as described in **Stereotactic injection** but at a speed of 30 nl/min. Immediately following AAV injection, 300 nL of *CAV2-FLEx-Flp* was injected into the MPA or VMHd at a speed of 100 nl/min using the stereotactic coordinates described above. In the control experiment where the *vGluT2-Cre*+ neurons were indiscriminately labeled, 1:5 mixture of *CAV2-FLEx-Flp* and AAV9 *hSyp-FLEx^{FRT}-mGFP-2a-SypRuby* (in total 100 nl) was injected into the MeA. The animals were sacrificed one month after the viral injections, and brain sections (obtained as described in Histochemistry) were stained with anti-GFP and anti-mCherry antibodies. Three to five images were taken from 30-μm coronal section (every 4th section) in each of the 8 brain regions (AOB, BNST, MPA, AHA, VMHd, VMHvl, PMCo, and PAGd) with a 10x objective using an Olympus epifluorescence microscope (BX53) equipped with ORCA-R2 cooled CCD camera (Hamamatsu Photonics). The field of view for each image was located based solely on DAPI staining so the experimenter was blind to the intensity of mGFP+ and SypRuby signals before imaging. In addition, 30-μm coronal sections (every 4th section) covering MeA area were imaged with a 4x objective to locate the source cells (defined by the expression of mGFP). We first counted the number of the source cells in MeAa, MeApd, MeApv and outside areas. Samples that contain more than 15% of total source cells located outside of the MeA were excluded from further analysis. We then cropped a 375 × 375 μm area for mGFP channel of each image and binarized it by using ImageJ, after thresholding to a value defined for each animal based on the most intensively labeled brain areas. The pixel densities of these binary images were measured and averaged to determine the fraction of mGFP+ axons originated from MeA *vGluT2*+ neurons in each brain region normalized by the total mGFP+ axons quantified from all 8 imaged regions in that brain.

To quantify the SypRuby+ dots in the VMH and MPA images, we first adjusted ImageJ parameters by using small number of images such that auto-detection of dots approximately matched to human-based count (data not shown). We cropped a 375 × 375 μm area for the SypRuby channels of each image and binarized it by ImageJ with default auto-adjustment thresholding cutoff value. We then used "analyze particle" function of ImageJ with pixel area 4–100 and circuity 0.5–1.0. We noticed that this method tends to underestimate the number of SypRuby+ dots when the axon density is high.

For the axon-initiated circuit mapping of *SF1*+ neuron (Figure S7), we performed the same experiments as MeA, but used *SF1-Cre* female mice injected with AAV9 *hSyp-FLEx^{FRT}-mGFP-2a-SypRuby* into the VMHd, and *CAV2-FLEx-Flp* into the either MPA or PAGd. In the control experiment in which *SF1-Cre* + neurons were indiscriminately labeled, 1:5 mixture of *CAV2* and AAV was injected into

the VMHd. Three to five images were taken from 30-μm coronal section (every 4th section) in each of the 11 brain regions (Sept, BNST, MPA, MeA, VMHd, VMHvl, PMCo, Rapir, SN, SubB, and PAGd) and analyzed as mentioned earlier for mGFP distribution.

Production of Recombinant ESP1

Recombinant ESP1 was produced as described previously (Kimoto et al., 2005). An expression vector *pET-28a* (Novagen, cat#69864) with the ESP1 sequence was transformed into *E. coli* BL21 (DE3). A mix of crude proteins was collected from bacterial pellets by sonication. ESP1 was purified from the protein mixture by HPLC fractionation in an anion-exchange DEAE-5PW column followed with C4 column, and finally re-suspended in 20 mM Tris-HCl pH 7.5. Solutions which were confirmed to induce cFos expression in the AOB were used for further experiments. ESP1 was soaked in cotton swab and dried for 4–5 hr before use.

Histochemistry

Mice were anesthetized with lethal amount of sodium pentobarbital, sacrificed and perfused with PBS followed by 4% PFA in PBS. The brain tissues were post-fixed with 4% PFA overnight, treated with 30% sucrose in PBS over two nights, and embedded in the O.C.T. compound (Tissue-Tek, cat#4583). Twenty to thirty-micron coronal brain sections were made using a Cryostat (Leica).

Fluorescent *in situ* hybridization (ISH) was performed based on TAI-FISH (Xiu et al., 2014) with some modifications. To make ISH probes, except the probe for *V2Rp5*, 650–1000 base pair DNA fragments containing the coding or untranslated region were amplified by PCR from the mouse whole brain cDNA (GenoStaff, cat#MD01) and cloned into pCR-BluntII-topo vector (Life Technologies, cat# K2800-20) for storage. DNA templates for intron probes (see below) were amplified by PCR from the C57BL/6 mouse genome. T3 RNA polymerase recognition site (5′-*AATTAACCCTCACTAAAGGG*) was added to the 3′ end of the PCR product. Primer sets used in the present study are shown in the Table S1.

DNA templates (500–1000 ng) were amplified by PCR, purified by PCR purification kit (QIAGEN, cat#28104), and then subjected to in vitro transcription with DIG- (cat#11277073910) or Flu (cat#11685619910)-RNA labeling mix and T3 RNA polymerase (cat#11031163001) according to the manufacture's instruction (Roche Applied Science). After DNase I (Roche Applied Science, cat#04716728001) treatment for 20 min at 37°C, the RNA probe was purified by ProbeQuant G-50 Columns (GE Healthcare, cat#28-9034-08). When possible, two or three independent RNA probes for the same gene were mixed.

Thirty micron coronal sections containing the target brain region were washed with PBS and treated with 10 μg/ml of protease K (Thermo Fisher Scientific cat#25530049) in 10 mM Tris-Cl (pH 7.4) and 1 mM EDTA (pH 8.0) for 10 min at 37°C. The sections were fixed with 4% PFA in PBS for 10 min and washed with PBS for 5 min, followed by acetylation with 0.25% acetic anhydride in 1.3% triethanolamine and 0.25% HCl for 10 min. After final wash with PBS for 5 min, the slides were dried.

RNA probe mixes (50–100 ng/μl) was diluted in a ratio of 1:100–1:200 into the hybridization buffer [50% formamide (Sigma-Aldrich cat#F9037), 0.6 M NaCl, 10 mM Tris-Cl (pH 8.0, Life Technologies cat#15568-025), 5 mM EDTA (Life Technologies cat#AM9260G), 0.3 mg/ml yeast-tRNA (Life Technologies cat#15401-029), 1x Denhalt's solution (Life Technologies cat#750018), 0.1 mg/ml Heparin (Sigma-Aldrich cat#H4784), 0.1% Tween-20, 0.25% SDS diluted into DEPC-treated ddW], mixed well, preheated at 85°C for 5 min, and immediately cooled down on ice. Probe containing hybridization buffer (200 μl) was applied to each slide on which the parafilm cover was placed. After 16h of incubation at 60°C in the moisture chamber with 50% formamide, the sections were washed, first with 2 × SSC-50% formamide, then with 2 × SSC, and finally with 0.2 × SSC twice for 20 min at 65°C.

For single color ISH, after blocking for 1h with 1% blocking buffer (Roche Applied Science, cat#10057177103 in 100 mM maleic acid adjusted pH to 8.0 with NaOH, 150 mM NaCl, 0.3% Tween-20), sections were incubated with horseradish peroxidase (HRP) conjugated anti-Dig antibody (Roche Applied Science cat#11207733910, 1:500 in blocking buffer) overnight at 4°C. On the next day, sections were washed three times with PBST for 10 min and treated with TSA-plus Cyanine 3 (PerkinElmer, NEL744001KT, 1:70 in 1x plus amplification diluent) for 20 min. Sections were washed once with PBST for 10 min, treated with PBS containing 50 ng/ml 4',6-diamidino-2-phenylindole dihydrochloride (DAPI, Sigma-Aldrich, cat#D8417) for 20 min, rinsed with PBS, and mounted with cover glass using Fluoromount (Diagnostic BioSystems cat#K024).

For two-color ISH, after blocking as mentioned above, sections were incubated with anti-Flu antibody (PerkinElmer NEF710001EA, 1:250 in blocking buffer) overnight at 4°C. On the next day, the sections were washed three times with PBST for 10 min, and treated with TSA-plus biotin (PerkinElmer, NEL749A001KT, 1:70 in 1x plus amplification diluent) at room temperature for 20 min. After washing with PBST for 5 min, HRP was inactivated with 2% sodium azide in PBS for 15 min, followed by 10 min wash three times with PBST. The sections were then incubated with HRP conjugated anti-DIG antibody (1:500 in blocking buffer) and streptavidin-Alexa Fluor 488 (Life Technologies, 1:250) overnight at 4°C. On the third day, sections were washed three times with PBST for 10 min and treated with TSA-plus Cyanine 3 (1:70 in 1x plus amplification diluent) or TSA-plus Cyanine 5 (1:100 in 1x plus amplification diluent, only for Figures S2G and S2H) for 20 min. Sections were washed once with PBST for 10 min, treated with PBS containing 50 ng/ml DAPI for 20 min and mounted with cover glass using Fluoromount (Diagnostic BioSystems cat#K024).

For immunohistochemistry, sections were washed three times with PBST for 10 min, and treated with 5% bovine serum albumin (BSA, Sigma-Aldrich) in PBST for 1 hr at room temperature for blocking. Sections were then incubated with anti-cFos (Santa Cruz Biotechnology, cat#sc-52-g, 1:200), anti-mCherry (Life technology cat#M11217, 1:500–1:1000), or anti-GFP (Aves Labs cat#GFP-1020, 1:500) diluted into 5% BSA in PBST for 3h at room temperature or overnight at 4°C. Signal positive cells were detected by anti-rat Cy3 (Millipore, cat#AP189C, 1:250), anti-chicken Alexa Fluor 488 (Invitrogen, cat#A11039, 1:250), anti-goat Alexa 488 (Invitrogen, cat#A11055, 1:250) diluted into PBST for 2h at room temperature or for overnight at 4°C. Sections were washed once

with PBST for 10 min, treated with PBS containing DAPI for 20 min, rinsed with PBS, and mounted with cover glass using Fluoromount (Diagnostic BioSystems cat#K024).

Sections were imaged by Olympus BX53 microscope (4x or 10x objective) equipped with ORCA-R2 cooled CCD camera (Hamamatsu Photonics). Images were processed in ImageJ and in Photoshop CS2 or 4 (Adobe).

cFos Mapping and catFISH

For *cFos* mapping experiments (Figures 3A, 3B, 5D–5G, 6A, 6B, and S2A–S2F), 8-week old C57BL/6 mice were singly housed for a week. Mice were exposed to 20 μg of ESP1 in cotton swab, 2-3 cm^2 of snakeskin (*Elaphe climacophora* shedding, Japan Snake Center), or control 10 mM Tris-Cl pH 7.5 buffer 20–30 min before sacrifice, 7–9 hr after the onset of their light period. In the MeA, every second coronal section (30-μm) was analyzed for *cFos* mRNA expression by single color FISH method. In the VMH, every second coronal section (30-μm) was stained with *SF1* (red) and *cFos* (green) by two-color ISH method.

To assess *cFos* induction in retrobeads+ MeApv neurons (Figures 3E–3G and S5A), 8-week old C57BL/6 mice were singly housed following red Retrobeads injection. Mice were exposed to ESP1, snakeskin or control buffer 30 min before sacrifice, 0.5–2 hr after the onset of their dark period. Only animals with injection near the correct coordinate were used for further analysis. In the MeA, every third coronal section (20-μm) were analyzed for Retrobeads and *cFos* mRNA expression by single color ISH method. To detect cFos+ cells in green, TSA-plus biotin (PerkinElmer, California, USA, NEL749A001KT) and streptavidin-Alexa Fluor 488 (Life Technologies, California, USA, 1:250) were used.

For cFos antibody staining (Figures S6A–E), mice were exposed to ESP1 90 min before sacrifice, 1.5–3 hr after the onset of their dark period. In the VMH, every third coronal section (20 μm) was analyzed for cFos and mCherry expression by double color IHC method.

To prepare samples for catFISH analysis (Figures 7A, 7B, and S5C–S5F), 8-week-old C57BL/6 mice were singly housed for a week. Stimulation was applied 7–9 hr after the onset of their light period. Two stimulants were applied to their home cages, each for 5 min and separated by 40 min. For example, in the 'ESP1-snake' sample, 20 μg ESP1 in cotton swab was placed into the cage. The cotton was carefully removed from the cage 5 min after the animal grabbed the cotton. 40 min after removal of ESP1, snakeskin was placed into the same cage. 5 min after the animal sensed the second stimulation, the mouse was quickly anesthetized with lethal amount of sodium pentobarbital and perfused directly with 4% PFA in PBS. Dissection was completed within 5 min to prevent the second stimulation from causing mature mRNA accumulation in the cytoplasm. Thirty-micron sagittal sections of the AOB and coronal sections of the MeA and VMH were analyzed by dual color ISH method as mentioned above. For MeA and VMH (Figures 7A and S5E), we selected an immediate early gene *NR4a1* based on pilot experiments (data not shown). We have confirmed that nearly 90% of *cFos*+ cells co-expressed *NR4a1* after ESP1 stimulation in the MeA and VMH. Dig-labeled *NR4a1*intron probe and Flu-labeled *NR4a1* coding probe mix (both about 1 ng/ml in the final concentration) were used for the hybridization. For the AOB (Figure S5C), we used Dig-labeled *cFos* intron probe (about 0.05 ng/ml in the final concentration) and Flu-labeled *cFos* coding probe mix (about 1 ng/ml in the final concentration) for the hybridization. Five to eight coronal sections containing AOB, MeApv, or VMHd were analyzed to count nuclear transcript (dots) positive cells, cytoplasmic mRNA positive cells, and dual positive cells. We noticed that when the same stimulant was given twice (e.g., "ESP1-ESP1") the nuclear transcripts positive cells (the second-stimulant responding cells) were reliably labeled with cytoplasmic mRNA (the first-stimulant responding cells), but many mRNA positive cells were not labeled with nuclear transcripts. Habituation to the same stimulation during the second application period, or less stable nature of induction of nuclear transcript may account for this observation. Whatever the mechanisms, we quantified the number of dual positive cells divided by the nuclear transcript positive cells (A-index in Figures 7B, S5D, and S5F) as readout of overlap in the neural representations. Of note, previous studies also used the same index (Lin et al., 2011; Wu et al., 2014)

TRAP

TRAP method was conducted as previously described with modifications (Guenthner et al., 2013). We selected *Arc-CreER* mice as a TRAP tool over *cFos-CreER* mice based on a pilot experiment (data not shown). *Arc-CreER* female mice were AAV injected followed by OVX and isolation. On the 5^{th} and 6^{th} day after isolation, animals were I.P. injected with 0.1 mL of corn oil at 7–8 hr after the onset of light period and were exposed to a piece of cotton in home cage 6 hr after the injection of corn oil. This process was conducted to habituate the animal and reduce background activity induced by I.P. injection and stimulation. On the 7^{th} day after isolation, animals were I.P. injected with 0.1 mL of tamoxifen (Sigma-Aldrich, 20 mg/ml) dissolved in corn oil at 7–8 hr after the onset of light period and were exposed to the stimuli in home cage 6 hr after the injection of tamoxifen. The stimulants were kept in home cage overnight. On the following day, mice were returned to the regular housing. Of note, control experiments omitting tamoxifen resulted in no Cre-dependent expression of a marker gene from a viral vector (data not shown).

As tamoxifen targets ER, we tested the possibility that tamoxifen application may alter representation of ESP1 in the VMH. Female mice that had i.p. injected with tamoxifen 6 hr before ESP1 stimulation showed no major difference in the number and distribution of cFos+ cells within the MeA and VMHd sub-regions compared to data from animals without tamoxifen (data not shown). This observation suggests that tamoxifen does not affect at least global representation of ESP1 in these regions.

Rabies *Trans*-synaptic Tracing

Preparation of rabies virus used in Figure 8E was conducted by using the viruses and cell lines as previously described (Osakada and Callaway, 2013). RV*dG-GFP* (a gift from Dr. Yamaguchi (University of Tokyo)) was amplified by using B7GG cell line (a gift from Dr. Callaway (Salk Institute)). Approximately 1.5 × 10^8 BHK-EnvA cells (a gift from Dr. Callaway, cultured in 5 × 225 cm^2 flasks) were infected with about 1 × 10^8 infectious particle of RV*dG-GFP*. Four hours after the infection, the cells were treated with Trypsin-EDTA, 0.25% (Life technologies #25200) to remove non-pseudotyped *RVdG-GFP* and re-plated into 5 × 225 cm^2 flasks. 4–5 days after the infection, the supernatant was collected, filtered with a 0.45-μm filter (Millipore cat#SE1M 003 M0), and concentrated by two-round of ultracentrifugation, first by Beckman SW28 rotor at 19,600 rpm for 2 hr and second by SW55 rotor at 21,000 rpm for 2 hr. The EnvA-pseudotyped RV*dG*-GFP+EnvA titer was estimated to be 1 × 10^9 infectious particles/ml based on serial dilutions of the virus stock followed by infection of the HEK293-TVA800 cell line (a gift from Dr. Callaway).

For *trans*-synaptic tracing using rabies virus, about 150 nL of 1:1 mixture of AAV2 *CAG-FLEx-TCb* and *CAG-FLEx-RG* (Miyamichi et al., 2013) was injected into the PAGd of *Esr1-Cre* female mice. To increase the number of starter cells, we injected AAVs into two sites along the lateral medial axis of the PAGd: one along the Midline, V 1.5 mm from the brain surface, and one in L 0.6 mm, V 1.75 mm, both above the Lambda along the anterior-posterior axis. Two weeks later, 150 nL of Rabies *dG-GFP*+EnvA was injected into the same brain region to initiate *trans*-synaptic tracing. Thirty-micron serial coronal sections throughout the brain were collected and every 4^{th} section around VMH area was subjected to dual color ISH analysis with *GFP* and *SF1* probes. Number of *SF1*+ GFP+ cells, *SF1*- GFP+ cells in the VMHd and GFP+ cells in the VMHvl (they are all *SF1*-negative) were counted, as well as the number of starter cells in the PAGd that were labeled with both GFP from rabies virus and mCherry form AAV *CAG-FLEx-TCb*.

Cell count

In histological analysis, cells were counted manually. For data shown by "per sections," 3–7 random sections containing the target brain area were used for analysis. For data shown by "per area," all sections containing the area (4 sections for MeAa, 12 sections for MeApd and MeApv, and 16 sections for VMH) were used. For data shown by "per unilateral MeA," 2 sections for MeAa, 5 sections for MeApd and MeApv were used. For data shown by "per mm^2," the number of cells was divided by area calculated using ImageJ software.

Schematic images

The schematic brain images used in Figures 2A, 5A, 6C, 6G, 7C, 7F, 8I, 8K, S1B, S2B, S4A, S6F, and S8C–S8F, were modified from AI files of brain atlas (Franklin and Paxinos, 2007).

QUANTIFICATION AND STATISTICAL ANALYSIS

To determine the number of animals required for ESP1-induced behavioral experiments, we conducted a power analysis using the variance calculated from pooled lordosis data of intact mice. These data were pooled from control animals in each experiment (for example, animals with GFP control virus injected, saline injected, etc.). For n = 65 pooled data, the lordosis percentage after ESP1 exposure was 41 ± 13%, and 12 ± 7.6% after control exposure (mean ± s.d.). Within this population, we found that 4.5 animals were sufficient to detect the difference ($p < 0.05$, power = 0.8) between average lordosis percentage of control (12%) and ESP1 (41%) stimulated animals in Students t test.

Data were presented as mean ± s.e.m. unless otherwise mentioned. The statistical details of each experiments including the statistical tests used, exact value of n and what n represents, are shown in each figure legend. For each statistical tests, unpaired Student's t test was used for Figures 3G, 5E, 5G, S4D, S4E, S5A, S5B, and S6I, and for multiple comparisons Bonferroni correction in Figures 3B and 6B. Paired Student's t test was used for Figure 8L, and for multiple comparisons with Bonferroni correction in Figures 2D, 5I, 6J, 7D, 7G, 8J, and S4G. Unrepeated one-way ANOVA was used for Figures 6F, 7B, S5D, S5F, and S6C–S6E with Bonferroni correction. Repeated one-way ANOVA was used for Figures 8C and 8D with Bonferroni correction. 95% confidence interval was used to determine significance. Significance was shown as $^*p < 0.05$, $^{**}p < 0.01$, and not significant values were not noted or shown as n.s.